The Canadian Journal of Chemical Engineering

formerly

CANADIAN JOURNAL OF TECHNOLOGY

CONTENTS

Heat Transfer in Water Spouted Beds	*B. Ghosh* *G. L. Osberg*	**205**
Influence of the Presence of Vapor Diffusion from a Wetted Non-Adiabatic Boundary upon the Sensible Heat Transfer Between a Boundary Wall and a Gas Stream	*C. P. Hedlin* *F. C. Hooper*	**208**
The Carbon Dioxide-Hydrogen Sulphide-Methane System. Part II: Phase Behavior at 40°F. and 160°F.	*D. B. Robinson* *A. P. Lorenzo* *C. A. Macrygeorgos*	**212**
Liquid-Liquid Extraction with Association Effects	*J. D. Raal* *A. I. Johnson*	**218**
Fundamental Aspects of Solids-Gas Flow. Part III: Accelerated Motion of a Particle in a Fluid	*L. B. Torobin* *W. H. Gauvin*	**224**
Index of Authors—1959		
Index of Articles—1959		

A Pigmy Paper-maker

turns out samples at the C-I-L Central Research Laboratory at Beloeil, Que. The products of this miniature paper mill are used to study bleaching of various types of wood pulp with C-I-L chemicals. The findings of the studies are made available to the pulp and paper industry through the technical service representatives of C-I-L.

C-I-L research helps many other industries to develop the improved products Canada needs for progress.

C-I-L

CANADIAN INDUSTRIES LIMITED

Serving Canadians Through Chemistry

Agricultural Chemicals • Ammunition • Coated Fabrics – Industrial Chemicals • Commercial Explosives • Paints • Plastics • Textile Fibres

The Canadian Journal of Chemical Engineering

formerly

Canadian Journal of Technology

VOLUME 37 DECEMBER, 1959 NUMBER 6

Authorized as second class mail, Post Office Department, Ottawa. Printed in Canada

Manuscripts for publication should be submitted to the Editor: Dr. A. Cholette, Faculty of Science, Laval University, Boulevard de l'Entente, Quebec, Que. (Instructions to authors are on the next page).

Editorial, Production and Circulation Offices: 18 Rideau Street, Ottawa 2, Ont.

Advertising Office: C. N. McCuaig, manager of advertising sales, *The Canadian Journal of Chemical Engineering*, Room 601, 217 Bay Street, Toronto, Ont. Telephone—EMpire 3-3871.

Plates and Advertising Copy: Send to *The Canadian Journal of Chemical Engineering*, 18 Rideau Street, Ottawa 2, Ont.

Subscription Rates: In Canada—$3.00 per year and 75c per single copy; U.S. and U.K.—$4.00; Foreign—$4.50.

Change of Address: Advise Circulation Department in advance of change of address, providing old as well as new address. Enclose address label if possible.

The Canadian Journal of Chemical Engineering is published by The Chemical Institute of Canada every two months.

The Canadian Journal of Chemical Engineering

INSTRUCTIONS TO AUTHORS

Manuscript Requirements for Articles

1. The manuscript should be in English or French.
2. The original and two copies of the manuscript should be supplied. These are to be on 8½ x 11 inch sheets, typewritten, and double spaced. Each page should be numbered.
3. Symbols should conform to American Standards Association. An abridged set of acceptable symbols is found in the third edition of Perry's Chemical Engineers' Handbook. Greek letters and subscripts and superscripts should be carefully made.
4. Abstracts of not more than 200 words in English indicating the scope of the work and the principal findings should accompany all technical papers.
5. References should be listed in the order in which they occur in the paper, after the text, using the form shown here: "Othmer, D. F., Jacobs, Jr., J. J., and Levy, J. F., Ind. Eng. Chem. **34**, 286 (1942). Abbreviations of journal names should conform to the "List of Periodicals Abstracted by Chemical Abstracts". Abbreviations of the common journals are to be found in Perry's Handbook also. All references should be carefully checked with the original article.
6. Tables should be numbered in Arabic numerals. They should have brief descriptive titles and should be appended to the paper. Column headings should be brief. Tables should contain a minimum of descriptive material.
7. All figures should be numbered from 1 up, in Arabic numerals. Drawings should be carefully made with India ink on white drawing paper or tracing linen. All lines should be of sufficient thickness to reproduce well, especially if the figure is to be reduced. Letters and numerals should be carefully and neatly made, with a stencil. Generally speaking, originals should not be more than twice the size of the desired reproduction; final engravings being 3¼ in. or 7 in. wide depending on whether one column or two is used.
8. Photographs should be made on glossy paper with strong contrasts. Photographs or groups of photographs should not be larger than three times the size of the desired reproduction.
9. All tables and figures should be referred to in the text.

Submission of Manuscripts

1. The three copies of the manuscript, including figures and tables, should be sent directly to:
   DR. A. CHOLETTE, editor,
   The Canadian Journal of Chemical Engineering,
   Faculty of Science, Laval University,
   Boulevard de l'Entente,
   Quebec, Que.
2. The authors addresses and titles should be submitted with the manuscript.
3. The author may suggest names of reviewers for his article, but the selection of the reviewers will be the responsibility of the editor. Each paper or article is to be reviewed by two chemical engineers familiar with the topic. Reviewers will remain anonymous.
4. All correspondence regarding reviews should be directed to the editor.

Reprints

1. At least 50 free "tear sheets" of each paper will be supplied.
2. Additional reprints may be purchased at cost. An estimated cost of reprints, with an attached order form, will be sent to the author with the galley proofs.
3. Orders for reprints must be made before the paper has appeared in the Journal.

Communications, Letters and Notes to the Editor

Short papers, as described below, will be considered for publication in this Journal. Their total length should not exceed 600 words, or its equivalent.

Communications

A communication is a prompt preliminary report of observations made which are judged to be sufficiently important to warrant expedited publication. It usually calls for a more expanded paper in which the original matter is republished with more details.

Letters

A letter consists of comments or remarks submitted by readers or authors in connection with previously published material. It may deal with various forms of discussion arising out of a publication or it may simply report and correct inadvertent errors.

Notes

A note is a short paper which describes a piece of work not sufficiently important or complete to make it worth a full article. It may refer to a study or piece of research which, while it is not finished and may not be finished, offers interesting aspects or facts. As in the case of an article a note is a final publication.

* * *

Heat Transfer in Water Spouted Beds[1]

B. GHOSH[2] and G. L. OSBERG[3]

Heat transfer from a column wall to water spouted sand beds was studied in a 9 in. diam. steel column. The heat transfer rate to water flowing through a spouted bed was lower than when the column was empty. The presence of a bed suppressed convection currents, causing a large temperature gradient from the wall to the centre of the bed, and consequently a lowered heat transfer rate. At the same water flow rate, the spouted bed gave a lower rate than a fixed bed, because a large fraction of the water bypassed the wall region and flowed up the spout.

In a previous communication from this laboratory on heat transfer from a column wall to a bed spouted with air, Klassen and Gishler (1) reported a sharp increase in the rate of heat transfer at the onset of spouting. They also obtained some preliminary data on wall to bed heat transfer in a water spouted system. Though there was an indication that the heat transfer rate decreased at the onset of spouting, the data were not sufficient for publication. The investigation was continued and the results are reported in the present communication.

Experimental

The heat transfer column, shown in Figure 1, consisted of two concentric steel cylinders: the inner one was 9 in. in diameter, 3/16 in. in thickness, and fitted with a 60° cone at the bottom, while the outer one was 12 in. in diameter, and 1/8 in. in thickness. The space between the cylinders was divided by two horizontal rings into three independent heating compartments. Steam superheated by approximately 10°F. was used for heating. The enthalpy of the condensate from each compartment was determined calorimetrically. The column and all pipings etc. were heavily insulated so as to make radiation and other heat loss corrections unnecessary.

Water was introduced at the bottom of the column through a half inch orifice. The water leaving the column contained no significant amounts of sand. It was thoroughly mixed in a tank, and its final temperature was determined before discharging it into the drain. The inlet and outlet temperatures of water were determined by mercury-in-glass thermometers.

Eight chromel-alumel thermocouples were embedded in the walls of the inner cylinder of the heat transfer apparatus, and five more were inserted into the column as floating thermocouples for exploring the radial temperature distribution at different levels.

Coarse, medium, and fine sands were used as bed materials. Physical properties of these are given in Table 1. At the beginning of a series of runs the column was filled with water and sand poured into it from the top to fill it up to predetermined stationary height. Water flow rate and the steam superheater were then adjusted, and when steady state was reached the heat transfer rate in each section was determined by calorimetric measurements, i.e. from a knowledge of the enthalpies of steam and condensate, and the rate of condensation. The total heat flow rate for the three sections was checked against that independently determined from the rate of water flow and the initial and final temperatures of water.

TABLE 1
PHYSICAL PROPERTIES OF BED MATERIALS

Material	Mesh size	Absolute density lb./cu.ft.	Bulk density lb./cu.ft.
Coarse sand.....	− 8 + 14	164	94.5
Medium sand.....	−14 + 20	160	91.5
Fine sand.....	−20 + 30	165	98.1

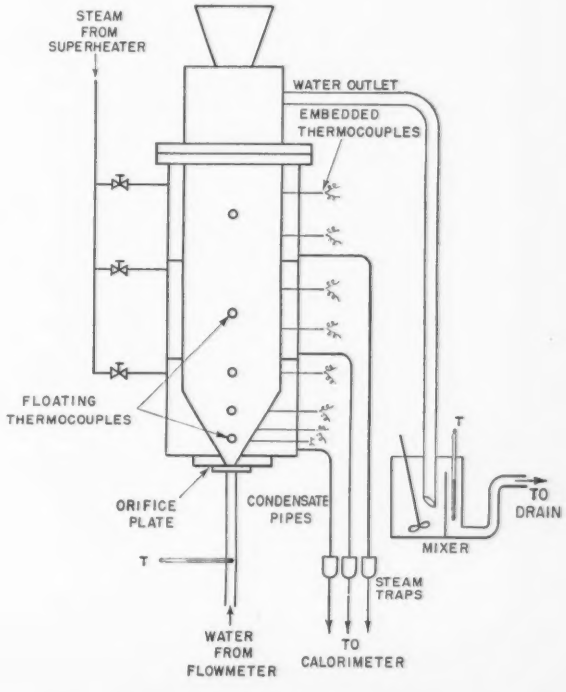

Figure 1—Heat transfer apparatus.

[1]*Manuscript received July 4, 1959.*
[2]*N.R.C. Post-doctorate Fellow. Present address: Department of Chemical Engineering, Jadavpur University, Calcutta-32, India.*
[3]*Division of Applied Chemistry, National Research Council, Ottawa, Ont.*
Contribution from the Division of Applied Chemistry, National Research Council, Ottawa, Ont. Issued as N.R.C. No. 5394.

The bed within the heat transfer column could not be visually observed. Hence, a 9 in. diam. glass column fitted with a 60° cone at the bottom and provided with a half inch water inlet was used for visual observation of the behavior of the bed at different water flow rates. Also, a plexiglass split column was used to observe the shape of the spout and to estimate the relative flow rates of water through the spout, and through the annulus surrounding the spout.

Data and Discussion

The heat transfer areas in the three sections starting from the bottom were respectively 1.70, 1.92, and 1.89 sq. ft. In the bottom section the cone provided 0.84 sq. ft. of heating surface and the rest of the surface was provided by the cylindrical portion of the column. However, no distinction was made between heat transferred through the conical and the cylindrical surfaces while calculating the average rates of heat transfer per unit area. Various bed heights were used, the maximum being 24 inches. A bed of this height covered the bottom and middle sections and a part of the top section of the column. The rate of heat transfer per unit area through the surface covered by the bed was approximately independent of bed height under spouting conditions. A typical set of data will be discussed in the following section.

The total rate of heat transfer in the bottom and the middle sections taken together, in B.t.u./hr., is plotted against water flow rate in Figure 2. These data refer to a bed height of 24 inches. The uppermost curve represents heat transfer from wall to water in absence of a bed, i.e. in an empty column. The presence of a bed diminished the rate of heat transfer considerably as shown by the lower curves. The lowermost curve represents heat transfer to a bed of fine sand, which spouted at the lowest water flow rate used. The next higher curve represents data on medium sand which did not start spouting until the flow rate represented by the point A was reached. Up to this point the bed remained stationary, and the rate of heat transferred from the column walls increased with increase in water flow rate. However, as soon as spouting started, the heat transfer rate decreased. Similiar trends were also exhibited by coarse sand which spouted at a water flow rate corresponding to the point B in Figure 2. It may be observed that the rate of heat transferred from column walls was relatively independent of particle size so long as the bed was spouting. For a static bed, however, the heat transfer rate increased with increasing particle size.

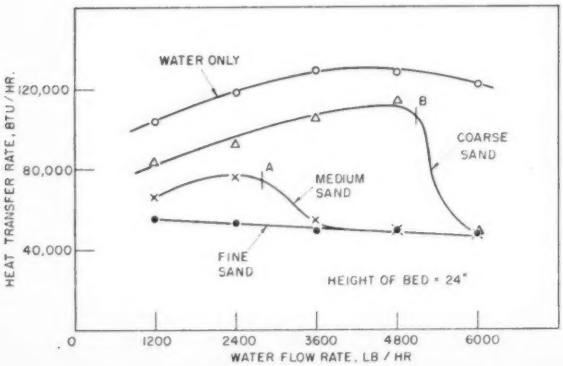

Figure 2—Total heat flow rate vs water flow rate.

It should be noted that the spout created turbulence in the region immediately above the bed. As water flow rates were increased, spout height, and induced turbulence also increased, so that at very high flow rates particles at the top of the bed fluidized. This fluidization caused an increase of 25-50% in the rate of heat transferred from the section in contact with the top part of the bed. For the data shown in Figure 2, however, the turbulent region affected only the upper section, and did not contribute to the heat transferred in the bottom and middle sections which are reported.

Heat transfer data are usually reported in terms of heat transfer coefficients calculated from the equation

$$h_{av} = \frac{q}{A(\Delta t)_{av}} \qquad (1)$$

The main difficulty in applying this equation to the spouted bed data is the selection of Δt, i.e. the average temperature difference between steam and the bed. In the absence of a bed convection currents obliterated temperature gradients except near the walls making it comparatively easy to determine a Δt. In the presence of a bed, however, convection currents were suppressed, and the temperature decreased gradually from the column wall to the center of the bed. This is evident from Figure 3 which shows a typical set of temperature readings across a horizontal section. It is difficult to obtain the average temperature of the bed at any cross-section from an integration of the corresponding temperature distribution curve since neither the composition of the water-sand mixture nor the flow rate of the mixture can be easily measured. Also, a continuous record of temperature at any point indicated rapid fluctuations. In the central portion of the column temperature fluctuations were about ± 0.5°C., while near the walls these were more than ± 15°C. (The points plotted in Figure 3 represent the time average temperatures at the corresponding points.)

Because of these circumstances, the overall temperature difference was obtained as follows. The inlet water temperature, and hence Δt at the inlet, i.e. at the bottom of the section under consideration was obtained by direct measurement. Since the bed remained confined within a section of the column, the total heat transferred through the walls was ultimately carried out of the section by the water flowing through the bed. The "mixing cup temperature" of the water leaving the section, and hence Δt at the top of the section under consideration, was obtained by calculation from the inlet water temperature, the water flow rate, and the rate of heat transferred in the section. An arithmetic average of the Δt's at the bottom and the top of the section was used in Equation (1) for calculating the average overall heat transfer coefficient.

A plot of h_{av} against flow rate is presented in Figure 4, using the same basic data as illustrated in Figure 2. Since the Δt's were different for different flow conditions the two figures, though similar, cannot be superimposed.

The heat transfer coefficient from steam to water flowing in a steam-jacketed vertical tube can be estimated from the natural convection equation recommended by McAdams [2] or by Colburn and Hougen [3]. Values calculated from these equations were approximately half of those obtained experimentally. Forced convection equations are not applicable in this case since N_{Re} and L/D are lower than the specified lower limits for which the equations apply [4]. The higher heat transfer coefficients observed in the present apparatus were probably due to the vigorous circulation of water induced by the high

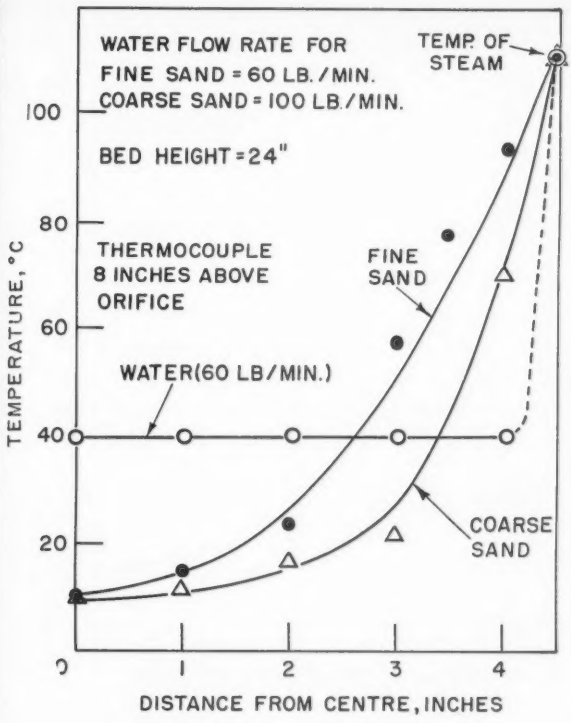

Figure 3—Temperature distribution.

velocity jet entering the column. These were relatively independent of flow rates (Figure 4).

Heat transfer characteristics of a water spouted bed are similar to those of a stirred slurry. An overall coefficient of 150-175 B.t.u./(hr.)(ft.^{2}) (°F.) has been reported by Laughlin [5] for transfer of heat from steam to a slurry of crystals in a jacketed cast iron vessel provided with a double scraper. For a water spouted bed the overall coefficients were of the order of 75-100 indicating a performance similar to that of a poorly stirred slurry.

Heat transfer studies by Richardson and Mitson [6] on water fluidized beds show that the heat transfer rate was more than doubled by the presence of a fluidized bed. Similar results were also reported by Caldas [7]. This increase in the rate of heat transfer has been ascribed to a reduction in the thickness of the laminar layer adjacent to the walls of the column, as well as to the extra turbulence created by the particles. In a water spouted bed, however, the heat transfer rate from wall to bed is considerably lower even though there is a scrubbing action of the particles against the walls. In a fluidized bed, there are no temperature gradients across the bed because of the rapid mixing within the bed, whereas in a spouted bed large temperature gradients are observed (Figure 3) showing that mixing and hence convective heat transfer within a water spouted bed is poor. It is the lack of convective currents which largely accounts for low rates of heat transfer in water spouted beds.

By analogy with water spouted beds one would also expect a suppression of convection currents in air spouted beds, and so it would appear anomalous that while a water spouted bed shows a decrease in the rate of heat transfer through the column walls at the onset of spouting, an air spouted bed shows a considerable increase.

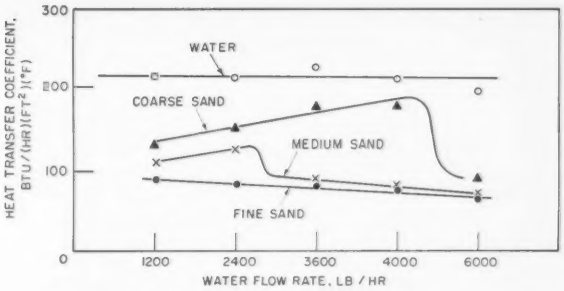

Figure 4—Heat transfer coefficient vs flow rate.

This may, however, be explained from the difference in the physical properties of air and water spouted beds. In the air spouted bed the heat capacity per unit volume is greatly increased by the presence of solids. For example, a sand air mixture containing 50% sand by volume has a heat capacity approximately 700 times that of air alone. It is known that this increase in heat capacity partially contributes to the rapid heat transfer in beds fluidized with air [8, 9]. Likewise, owing to the increased heat capacity, in an air spouted bed a considerable amount of heat is transferred from the solids to air by the circulation of solids at the onset of spouting, and this more than compensates the effect of suppression of convection currents within the bed. As a result the overall rate of heat transfer shows an increase. On the other hand, in a water spouted bed the heat capacity of the bed per unit volume is not very different from that of water. Hence, the effect of suppression of convection currents within the bed predominates, and the rate of heat transfer from wall to bed is considerably lowered. For the same water flow rate, however, the heat transfer rate from wall to a packed bed is higher than that in a spouted bed, because, in the latter a large fraction of the total flow, approximately 70-80%, passes through the spout. Consequently, the flow rate past the heating surface, and hence the heat transfer rate, is reduced at the onset of spouting. In view of the inefficiency of wall to bed heat transfer in a water spouted bed when compared with wall to bed heat transfer in a fixed or fluidized bed under similar water flow conditions, no attempt was made to develop empirical equations for correlating the data.

Acknowledgment

The authors thank T. W. Boyd for setting up the apparatus and rendering technical assistance throughout the investigation.

Nomenclature

h_{av} = average heat transfer coefficient
q = quantity of heat transferred per unit time
A = area of heat transfer surface
Δt = overall temperature difference
$(\Delta t)_{av}$ = average overall temperature difference
L = length of column
D = diameter of column
N_{Re} = Reynold's number

References

(1) Klassen, J., and Gishler, P. E., Can. J. Chem. Eng. 36, 12 (1958).
(2) McAdams, W. H., "Heat Transmission", p. 174, third edition, McGraw-Hill, 1954.
(3) Colburn, A. P. and Hougen, O. A., Ind. Eng. Chem. 22, 522 (1930).
(4) Knudsen, J. G., and Katz, D. L., "Fluid Dynamics and Heat Transfer", pp. 394-396, McGraw-Hill, 1958.
(5) Laughlin, H. G., Trans. A.I.Ch.E. 36, 345 (1940).
(6) Richardson, J. F., and Mitson, A. E., Trans. Inst. Chem. Eng. (London), 36, 270 (1958).
(7) Caldas, I., Ph.D. Thesis (1955), Cincinnati University.
(8) Dow, W. M., and Jakob, M., Chem. Eng. Progr. 47, 637 (1951).
(9) van Heerden, C., et al., "Proceedings of the General Discussion on Heat Transfer", pp. 358-360, 389, Institution of Mechanical Engineers, New York (1952).

★ ★ ★

Influence of the Presence of Vapor Diffusion from a Wetted Non-Adiabatic Boundary upon the Sensible Heat Transfer between a Boundary Wall and a Gas Stream[1]

C. P. HEDLIN[2] and F. C. HOOPER[3]

The evaporation of a liquid from a wetted surface into a gas stream has consequences which are of fundamental importance in the analysis of sensible heat transfer at the boundary. The presence of a relatively high concentration of vapor in the region adjacent to the surface influences the physical properties of the fluid and the vapor concentration gradient affects the heat transfer mechanism.

Experimental equipment was devised to measure the sensible heat transfer coefficients at the inside surface of a porous ceramic tube from which water was being evaporated. Series of tests were carried out for non-adiabatic wall conditions over ranges of the Reynolds Number from 5,600 to 16,000, tube diameter from 1.360 to 3.300 inches, bulk air temperature from 150 to 220°F., and wall vapor pressures from 0.35 to 2.20 p.s.i.a.

Over the range of vapor pressures and evaporation rates investigated, the sensible heat transfer coefficients were not observed to depart significantly from those predicted by generally accepted relationships for the dry wall case.

THE evaporation of a liquid from a wetted surface into a gas stream has consequences which are of fundamental importance in the analysis of sensible heat transfer in the boundary region. Individually, heat and mass transfer have been the subjects of extensive experimental investigation and analytical work but comparatively little attention has been paid to the influence of mass transfer on the transfer of sensible heat when they occur simultaneously in the same field.

Consideration of this combination of phenomena acting together suggests several factors of importance. The presence of a relatively high concentration of vapor in the region adjacent to the wetted surface influences the physical properties of the fluid and, therefore, affects the heat transfer mechanism. Secondly, the diffusion of mass through the boundary region results in a sensible fluid flow. This phenomenon, which was discovered by Stefan and studied further by Meyer and Thoma [1], affects the rate of sensible heat transfer. Thirdly, sensible heat is required to change the evaporated vapor to the gas stream temperature and thus a heat source or sink exists in this region with a consequent effect on sensible heat transfer at the boundary wall. Finally, the vapor must be accelerated to stream velocity and the resulting inertial force has been shown by Ackermann [2] to increase the thickness of the boundary layer and therefore to reduce the rate of sensible heat transfer.

Several investigators have developed expressions for sensible heat transfer which incorporate the mass transfer effects. Nusselt [3] derived an expression for sensible heat transfer between an evaporation surface and a gas stream of different temperature, by combining the expression for the secondary convective stream, caused by mass transfer, with a conventional expression for heat transfer at a dry surface. Spalding's theoretical work [4] on heat and mass transfer for fuel droplet combustion yields the expression

$$\frac{Nu}{Nu^*} = \frac{\ln(1 + B)}{B} \qquad (1)$$

where Nu and Nu* are, respectively, the Nusselt numbers with and without evaporation. For evaporation without combustion

$$B = \frac{c_p(T_g - T_s)}{Q}$$

where c_p is the specific heat of the vapor, T_g and T_s are respectively, the gas temperature and the droplet surface temperature, and Q is the latent heat of vaporization of the liquid. Godsave [5, 6] presented theoretical expressions for heat transfer between a flame front and the evaporating spherical fuel drop which the front encloses. These expressions, together with experimental data, are used to show that, for burning fuel drops, the Nusselt number decreases as the mass transfer rate increases. In formulating an expression for heat transfer for the case of condensation of mixed vapors, Colburn and Drew [7] included the sensible heat contributed by cooling the vapor to condensing temperature. Experimental heat trans-

[1] *Manuscript received July 31, 1959.*
[2] *Associate Professor, Department of Engineering Science, Ontario Agricultural College, Guelph, Ont.*
[3] *Assistant Professor of Mechanical Engineering, University of Toronto, Toronto, Ont.*
The work reported here was carried out in the laboratories of the Mechanical Engineering Department at the University of Toronto and was used by C. P. Hedlin in his doctoral thesis at that institution.

fer results were correlated by Ingebo [8] for adiabatic evaporation of nine different organic liquids from spheres using the Nu, Re, and Sc groups in the equation.

The analogy between heat and momentum transfer first proposed by Reynolds [9] and since extended by a number of workers including Von Karman [10] and Martinelli [9] facilitates analysis.

Molecular and eddy diffusion cause transport of fluid across a turbulent stream and, if a temperature differential exists, transfer of sensible heat also results. When the Prandtl number equals unity, the equation

$$\frac{h}{c_p G} = \frac{f}{2} \quad \ldots\ldots (2)$$

derived from the analogy of heat and momentum transfer, gives values that agree closely with experimental heat transfer results. Since a secondary convective stream apparently influences the sensible heat transfer for the wetted wall case, this concept is of particular interest and leads to a method of correlating heat transfer results.

For the case of a fluid stream flowing along a dry boundary wall, consider the rate of diffusion of the flowing fluid, normal to the direction of stream motion, (associated with momentum transfer at the wall) to be equivalent to a sensible flow having a velocity u_d at the wall. The acceleration of a quantity of fluid ρu_d to the average stream velocity u is accomplished in unit time and the drag per unit area of the wall is

$$F = \frac{\rho u_d u}{g_c} \quad \ldots\ldots (3)$$

but also

$$F = \frac{\frac{1}{2} f \rho u^2}{g_c} \quad \ldots\ldots (4)$$

therefore,

$$\tfrac{1}{2} f = \frac{u_d}{u} \quad \ldots\ldots (5)$$

Following McAdams' recommendation for sensible heat transfer,

$$\frac{h_L}{c_{pb} G} \left(\frac{c_p \mu}{k} \right)^{2/3} = \frac{0.023}{(DG/\mu)^{.2}} \quad \ldots\ldots (6)$$

and for the friction factor

$$f = 0.046/Re^{0.2} \quad \ldots\ldots (7)$$

one obtains

$$St\ Pr^{2/3} = \tfrac{1}{2} f = \frac{u_d}{u} \quad \ldots\ldots (8)$$

The transport of heat and momentum by the hypothetical sensible flow is therefore equivalent to that which actually results from molecular and eddy diffusion. In the particular case of heat and mass transfer at a wetted wall, a sensible flow of gas is caused by the vapor transfer and is added to the gas interchange that occurs for the dry wall case.

$$u_t = u_d + u_s \quad \ldots\ldots (9)$$

$$St\ Pr^{2/3} = 0.023/Re^{.2} + u_s/u \quad \ldots\ldots (10)$$

The assumption that

$$u_s = f(u, D, p, G_m, \nu, D_v, g_c) \text{ leads to} \quad \ldots\ldots (11)$$

$$u_s/u = \propto (uD/\nu)^a (D_v/\nu)^b \left(\frac{G_m u}{p g_c} \right)^c \quad \ldots\ldots (12)$$

If the constants in Equation (12) are evaluated empirically, the influence of previously mentioned factors arising from the mass transfer should be accounted for with the exception of the heat required to raise the vapor temperature to that of the fluid stream.

Equipment

Experimental equipment was designed and constructed to permit the evaluation of the sensible heat transfer at the inside surface of a tube through which a turbulent flow of heated air was passing while non-adiabatic evaporation of water took place from the surface into the air stream.

A system (Figure 1) consisting of a fan, a stilling tank with an adjustable waste opening, an orifice meter, electrical resistance heaters, and the necessary piping provided air at a controlled rate and temperature. Preceding its passage over the transfer surface, the air flowed along an approach pipe which functioned to reduce entry effects to an acceptable level [9]. A connection (Figure 2) provided for uninterrupted flow from the approach pipe into a porous ceramic tube. The inner surface of this tube was kept wet in the manner described below and the rates of sensible heat transfer and water evaporation at its inner surface were measured.

Porous ceramic, having a capillary potential of about 5 inches, formed the transfer surface. Tubes of this material, with a length-diameter ratio of approximately 1.6 were obtained in rough form and finished in a lathe to an inside diameter tolerance of $\pm$ 0.001 inch. From four to six of these tube sections were placed end to end in each transfer assembly, the end sections served as guards to minimize radiation and conduction from non-equilibrium areas to the measuring sections of the transfer surface.

It was necessary to supply water to each tube section separately, and of course, at a rate equal to the rate of evaporation from its surface. Two sumps were attached externally to each tube section; one around the top and the other around the bottom. During a test, water was supplied to the top sump at a rate which was kept somewhat less than the evaporation rate for the tube section. Water from this sump kept the upper portion of the tube section wet and water carried by capillary force from the bottom sump supplied the remainder of the surface. Teflon sheet of 0.005 inch thickness was used to form the sumps and to separate adjacent tube sections.

Chromel A resistance wire was wound around the tube sections so that heat could be supplied at a controlled rate to the inner surface to control the transfer surface temperature and indirectly the evaporation rate. The rate of heat loss to the surroundings from the transfer assembly was measured by enclosing the ceramic tubes in a polyethylene tube with a thermopile placed across the wall and using this tube as a heat meter.

Since it was not possible to make a direct measurement of the temperature of the transfer surface without causing undesirable roughness, thermocouples were located by drilling two holes in the tube wall parallel to the axis of the tube and in the same axial plane. One thermocouple, enclosed in a small glass tube to prevent corrosion, was placed in each hole. By extrapolation on a temperature-position plot, it was possible to determine the temperature of the inside surface adjacent to each pair of thermocouples.

The completed assembly, consisting of the components described above, is referred to as the transfer assembly

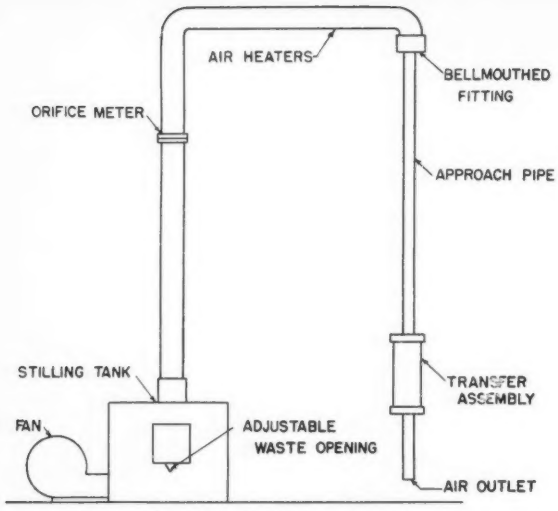

Figure 1—Overall diagram of equipment.

(Figure 2). With this equipment it was possible to measure the rate of water evaporation from each tube section separately, and by measuring directly the heat supplied by the heaters to obtain by difference the heat transferred from the air to the transfer surface.

When a test was made, it was necessary to operate the equipment for one to two hours before completely stable conditions were obtained at the transfer surface. After establishment of equilibrium the water consumption was carefully measured for two to four hours and this value, together with other measured variables, was used to compute the sensible heat transfer coefficient.

Results

Analysis of the results required the evaluation of the physical properties of the fluid. It was necessary to consider the influence, not only of temperature, but also of the vapor in the boundary region on the viscosity, density, specific heat and thermal conductivity.

The problem of extending the validity of equations to include cases where fluid properties are not uniform in the boundary region has been studied by a number of investigators. Nusselt [11] showed that a particular equation has general validity for gases when logarithmic mean values of the wall and bulk stream properties were used. Other results [9] obtained with large temperature differences across the boundary layer, were successfully correlated when arithmetic mean values of the bulk and wall temperatures were used. In the work reported here, arithmetic mean values of the temperatures and vapor pressures were used as the basis for calculating the physical properties of the fluid stream.

The viscosity was calculated using the relationship of Buddenberg and Wilke [12]. Thermal conductivities were obtained from tables, and specific heats and densities were calculated by assuming that the influence of the vapor was directly proportional to its concentration.

Difficulties were experienced from the deposition of foreign material at the transfer surface and this often resulted in the existence of a vapor pressure that was less than the saturation vapor pressure for water at the existing wall temperature. For this reason, it was necessary to determine the vapor pressure on the basis of other measured variables. The mass transfer coefficient was calculated [9] and the corresponding vapor pressure difference was then evaluated using the known rate of mass transfer.

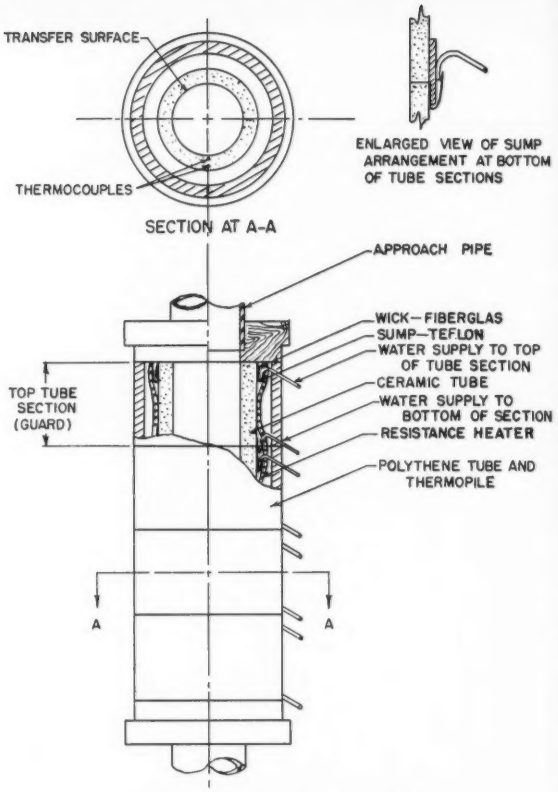

Figure 2—Transfer assembly.

Seventy-six observations of the heat transfer coefficient were made in the ranges of the variables shown in Table 1.

The quantity u_s/u (Equation (8)) was calculated for each observation. In all cases these values were small compared to St $Pr^{2/3}$, ranging from −0.00098 to 0.00143 (Figure 3). There were equal numbers of positive and negative values; the average of the positive values was 0.00028 and the average of the negative values was −0.00045.

Attempts were made to discover a systematic influence on this quantity on the heat transfer factor, St $Pr^{2/3}$. A

TABLE 1

Variable	Range	Variable	Range
Re	5600 to 16000	ρ_f	0.0595 to 0.0691 lb. mass/ft.^{3}
D	0.1133 to 0.2750 ft.	k_f	0.0159 to 0.0176 B.T.U./(hr.)(ft.)(°F)
G_m	0.17 to 1.61 lb. mass/(hr.)(ft.^{2})	p	1912 to 2066 lbs./ft.^{2}
T_w	90 to 140°F.	u	20,000 to 110,000 ft./hr.
p_w	0.35 to 2.16 p.s.i.a.	h	1.25 to 7.80 B.T.U./(hr.)(ft.^{2})(°F.)
μ_f	0.0437 to 0.0471 lb. mass/(hr.)(ft.)	T_a	160 to 220°F.

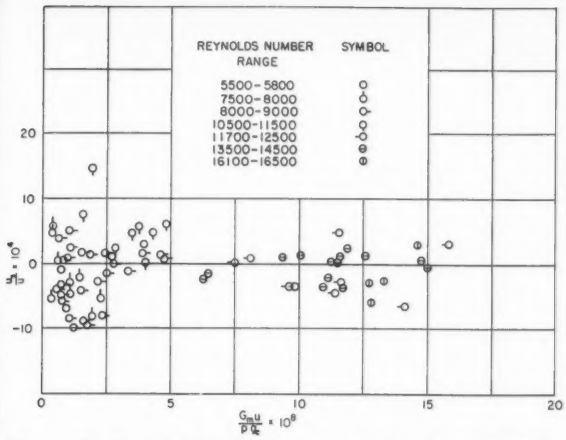

Figure 3—Graphical representation of experimental results.

statistical analysis, which employed the method of least squares, was conducted to fit a curve, based on Equation (12), to these values.

The variation of the Schmidt number was very small and it was assumed to be constant in the analysis.

Inspection of the resulting equation indicated that it did not rationally account for a significant part of the variation in u_s/u. The same conclusion was reached with respect to equations of other dimensionless groups obtained from Equation (11). From this it was concluded that the experimental error accounted for the observed variation. This conclusion is supported by the closeness with which the experimental results for all rates of evaporation conform to Equation (6). The use of all the observations gives a value of 0.0226 for the multiplying constant in the latter equation in place of the generally accepted value of 0.023, and this value does not vary in a systematic manner when the experimental results are plotted against evaporation rate.

For a number of reasons this investigation was confined to the air-water combination and as a result is limited in generality. More general conclusions on the effect of mass transfer on sensible heat transfer must await similar work with several additional liquids of varied characteristics. Formulation of general relationships based on experimental evidence would require investigations over broader ranges of evaporation rates and gas-surface temperature differentials.

Conclusions

The influence of water vapor transfer on sensible heat transfer at a non-adiabatic wall is not significant in the ranges of variation of the variables investigated. The experimental results obtained in these ranges are satisfactorily correlated by equations that are applicable to similar dry wall cases.

This result tends to support to some extent the practice of workers in psychrometric and drying problems of ignoring the effects of heat and mass transfer upon one another when they occur together. It is by no means to be expected that the assumption of independence would retain its validity over broader ranges of the variables, and most particularly not at high mass transfer rates.

Nomenclature

A = area, ft.²
c_p = specific heat capacity at constant pressure, B.t.u./(lb.)(°F.); c_{pb} for bulk conditions; c_{pf} for film conditions.
D = inside tube diameter, ft.
D_v = mechanical diffusion, ft.²/hr.
f = friction factor.
F = shear stress, lb. force/ft.²
G = mass velocity of fluid, lb.mass/(hr.)(ft.² of tube cross section).
G_m = evaporation rate, lb.mass/(hr.)(ft.² of tube wall).
g = acceleration due to gravity. ft./hr.²
g_c = conversion factor (lb.mass)(ft.)/(lb.force)(hr.²).
h = heat transfer coefficient, B.t.u./(hr.)(ft.²)(°F.); h_L based on logarithmic mean temperature difference.
k = thermal conductivity, B.t.u./(hr.)(ft.)(°F.); k_f for film conditions.
T = temperature, °F.; T_w for transfer surface; T_a bulk temperature of air flowing over the transfer surface.
u = bulk fluid stream velocity, ft./hr. equivalent fluid velocity perpendicular to the boundary wall; u_d for the dry wall case; u_s for flow resulting from mass transfer; u_t for the general case, with or without mass transfer.
p = partial pressure of air, lb.force/ft.²
p_f = partial pressure of vapor for film conditions, p.s.i.a.
μ = absolute viscosity, lb.mass/(hr.)(ft.); μ_f for film conditions.
ν = kinematic viscosity, ft.²/hr.
ρ = density, lb.mass/ft.³; ρ_f for film conditions.
Nu = Nusselt number, hD/k.
Pr = Prandtl number $\mu c_p/k$.
Re = Reynolds number GD/ν.
Sc = Schmidt number D_v/ν.

References

(1) Jakob, M., Heat Transfer, Vol. 1, 598.
(2) Ackermann, G., V.D.I., Forschungsheft No. 382 (1937).
(3) Nusselt, W., Heat transfer, diffusion and evaporation, NACA TM 1367 (March 1954).
(4) Spalding, D. B., Fourth Symposium (International) on Combustion, 847, Baltimore, The Williams and Wilkins Co. (1953).
(5) Godsave, G. A. E., Fourth Symposium (International) on Combustion, 818.
(6) Godsave, G. A. E., Report No. R66, N.G.T.E., England, March 1950; Report No. R87, N.G.T.E., England, April 1951; Report No. R88, N.G.T.E., England, August 1952.
(7) Colburn, A. P., Drew, T. B., Trans. Am. Inst. Chem. Eng. 33, 197 (1937).
(8) Ingebo, R. D., NACA TN 2368 (July 1951).
(9) McAdams, W. H., Heat Transmission, 3d Ed.
(10) Jakob, M., Heat Transfer, Vol. 1, 504.
(11) Jakob, M., Heat Transfer, Vol. 1, 496.
(12) Buddenberg, J. W., Wilke, C. P., Ind. Eng. Chem. 41, 1345 (1949).

★ ★ ★

The Carbon Dioxide-Hydrogen Sulphide-Methane System

Part II. Phase Behavior at 40°F. and 160°F.[1]

D. B. ROBINSON[2], *A. P. LORENZO*[3] *and*
C. A. MACRYGEORGOS[4]

The phase behavior of the carbon dioxide-hydrogen sulphide-methane system, previously reported at a temperature of 100°F. (1), has been investigated at pressures of 400, 1000, and 1600 lb./in.²abs. at 40°F. and at pressures of 1000, 1330 and 1600 lb./in.²abs. at 160°F. Correlation of the experimental data is based upon equilibrium ratios calculated for the individual components. Equilibrium ratios were found to be a function of system composition, temperature, and pressure. Deviation of the liquid phase from ideal solution behavior, as indicated by calculated activity coefficient ratios, is, in general, most dependent upon system composition at the higher pressures and lower temperatures.

A MORE complete representation of vapor-liquid equilibrium in the ternary system carbon dioxide-hydrogen sulphide-methane has been achieved by extension of the study to both higher and lower temperatures than that previously investigated. Work has been carried out at a temperature nearer the maximum for which two phase equilibrium occurs in this three component system; and also at a temperature which is below the critical temperatures of both of the less volatile components so that vapor-liquid equilibrium occurs in all three of the binary systems. The present work permits prediction of the effect of pressure, temperature and system composition on the distribution of the components between the vapor and liquid phases and on the approach to ideality of the liquid solutions. Experimental techniques and analytical procedures discussed in Part I of this series were followed closely in this work.

Theory

Phase behavior in a ternary system may be adequately described by the construction of the series of isobaric, isothermal, triangular diagrams depicting the compositions of co-existing vapor and liquid phases. The experimental phase composition data is readily correlated by calculation of equilibrium ratios; while a comparison between the behavior of the real system and the behavior of an ideal solution may be made by calculation of activity coefficient ratios. The concepts of the equilibrium ratio and the activity coefficient ratio were discussed briefly in Part I of this series.

The activity coefficient ratio is defined by the equation:

$$\gamma_i = \frac{y_i}{x_i} \cdot \frac{f_v}{f_L^*}$$

while the experimental equilibrium ratio is defined by the equation:

$$K_{i\,Exp.} = \frac{y_i}{x_i} = \gamma_i \cdot \frac{f_L^*}{f_v} = \gamma_i \cdot K_{i\,Theor.}$$

The general form of the isobaric, isothermal phase equilibrium diagrams for the ternary system may be predicted from a knowledge of the pressure-composition diagrams for the binary systems. Since the critical temperatures of hydrogen sulphide and carbon dioxide are above 40°F., at the lower temperature used in this study both of these components exist as liquids under the test conditions. Accordingly, vapor-liquid equilibrium occurs in all three binary systems—methane and hydrogen sulphide, carbon dioxide and hydrogen sulphide, methane and carbon dioxide. Data on the methane-hydrogen sulphide system at 40°F. have been reported by Reamer, Sage and Lacey (2); while data on the carbon dioxide-hydrogen sulphide system between the ice point and the circondentherm have been reported by Bierlein and Kay (3). Donnelly and Katz (4) have investigated phase equilibrium in the methane-carbon dioxide system up to a temperature of 29°F. which is below the minimum temperature investigated in this work.

At a temperature of 160°F. the system is above the critical temperature of both methane and carbon dioxide. Consequently two phase vapor-liquid equilibrium does not occur in the methane-carbon dioxide system. Reamer, Sage and Lacey (2) report data for the methane-hydrogen sulphide system at 160°F. Values for the carbon dioxide-hydrogen sulphide system at this temperature may be interpolated from the data of Bierlein and Kay (3).

[1]*Manuscript received August 5, 1959.*
[2]*Professor of Chemical Engineering, University of Alberta, Edmonton, Alta.*
[3]*Union Carbide Corp., Buffalo, N.Y.*
[4]*Canadian Chemical Co. Limited, Edmonton, Alta.*
Contribution from the Department of Chemical and Petroleum Engineering, University of Alberta, Edmonton, Alta.

Experimental Methods

The variable volume, visual type equilibrium cell and auxiliary apparatus described by Robinson and Bailey [1] was employed in this study. Modification of the equipment permitted extension of the temperature range over which phase behavior could be investigated. In the work at 160°, air was circulated over electrical heating coils and then through the constant temperature air bath surrounding the equilibrium cell. At a temperature of 40°F. the air was circulated in the same manner over a series of finned copper tubes carrying ethylene glycol which had been cooled by a standard vapor compression type of refrigeration system. Temperatures were held constant to within ± 0.2 degrees at both 40°F. and 160°F.

Experimental Results

The experimental data obtained at pressures of 400, 1000 and 1600 lb./in.² abs. at 40°F. and at pressures of 1000, 1330 and 1600 lb./in.² abs. at 160°F. are presented in Table 1. Figures 1 to 3 inclusive represent the corresponding ternary isobaric diagrams. In each case the intersections of the dew point and bubble point loci with the axes of the equilateral triangle represent respectively the vapor and liquid phase compositions of the binary systems. Close agreement between the experimental results and published values for the binary systems was obtained.

Figure 1 illustrates the phase equilibrium at a pressure between the vapor pressures of hydrogen sulphide and carbon dioxide at 40°F. and, hence, the two phase region

TABLE 1

EXPERIMENTAL PHASE COMPOSITION DATA

Test No.	Total System			Vapor Phase			Liquid Phase		
	H_2S	CO_2	CH_4	H_2S	CO_2	CH_4	H_2S	CO_2	CH_4
	Temperature = 40°F.					Pressure = 400 lbs/in.² abs.			
–	0.677	0.0	0.323	0.489	0.0	0.511	0.977	0.0	0.023
A–7	0.725	0.081	0.194	0.477	0.131	0.392	0.940	0.027	0.033
A–2	0.660	0.142	0.198	0.454	0.192	0.354	0.889	0.070	0.041
A–3	0.636	0.197	0.167	0.429	0.253	0.318	0.832	0.129	0.039
A–4	0.620	0.259	0.121	0.423	0.352	0.225	0.819	0.148	0.033
A–5	0.574	0.339	0.037	0.404	0.450	0.146	0.702	0.280	0.018
A–6	0.518	0.426	0.056	0.416	0.503	0.031	0.635	0.350	0.015
–	0.451	0.549	0.0	0.365	0.635	0.0	0.597	0.403	0.0
	Temperature = 40°F.					Pressure = 1000 lbs/in² abs.			
–	0.594	0.0	0.406	0.284	0.0	0.716	0.878	0.0	0.122
B–1	0.551	0.125	0.324	0.291	0.139	0.570	0.756	0.090	0.154
B–2	0.473	0.252	0.275	0.259	0.266	0.475	0.625	0.221	0.154
B–4	0.320	0.392	0.288	0.229	0.353	0.418	0.412	0.414	0.174
B–5	0.218	0.523	0.259	0.179	0.471	0.350	0.284	0.537	0.179
B–6	0.117	0.627	0.256	0.104	0.567	0.329	0.144	0.680	0.176
–	0.0	0.744	0.256	0.0	0.655	0.345	0.0	0.867	0.133
	Temperature = 40°F.					Pressure = 1600 lbs/in.² abs.			
–	0.526	0.0	0.474	0.292	0.0	0.708	0.744	0.0	0.256
C–2	0.444	0.089	0.467	0.311	0.087	0.602	0.643	0.063	0.294
C–3	0.437	0.155	0.408	0.340	0.142	0.518	0.488	0.135	0.377
C–4	0.388	0.175	0.437	Critical System Composition for 1600 lbs/in.² abs.					
	Temperature = 160°F.					Pressure = 1000 lbs/in.² abs.			
D–1	0.908	0.0	0.092	0.844	0.0	0.156	0.968	0.0	0.032
D–4	0.876	0.054	0.070	0.836	0.061	0.103	0.936	0.031	0.033
D–5	0.861	0.093	0.046	0.822	0.118	0.060	0.911	0.063	0.026
D–2	0.851	0.149	0.0	0.811	0.189	0.0	0.891	0.109	0.0
	Temperature = 160°F.					Pressure = 1330 lbs/in.² abs.			
F–1	0.811	0.048	0.141	0.724	0.066	0.210	0.903	0.023	0.074
F–2	0.732	0.109	0.159	0.704	0.126	0.170	0.848	0.064	0.088
F–3	0.703	0.155	0.142	0.699	0.162	0.139	0.770	0.123	0.107
F–4	0.696	0.203	0.101	0.676	0.224	0.100	0.718	0.197	0.085
F–5	0.691	0.218	0.090	Too unstable to sample					
F–6	0.657	0.250	0.093	Single Phase					
	Temperature = 160°F.					Pressure = 1600 lbs/in.² abs.			
E–1	0.784	0.0	0.216	0.735	0.0	0.265	0.841	0.0	0.159
E–3	0.769	0.028	0.203	0.737	0.027	0.236	0.818	0.018	0.164
E–2	0.755	0.051	0.194	Critical System Composition for 1600 lbs/in.² abs.					

All compositions are in mole fractions.

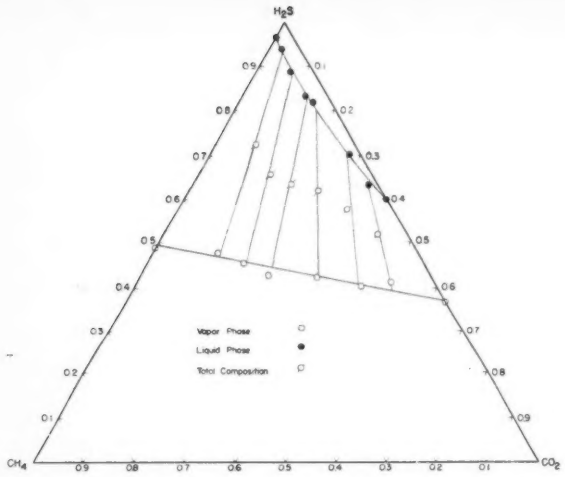

Figure 1 — Phase diagram at 40°F. and 400 lb./in.² abs.

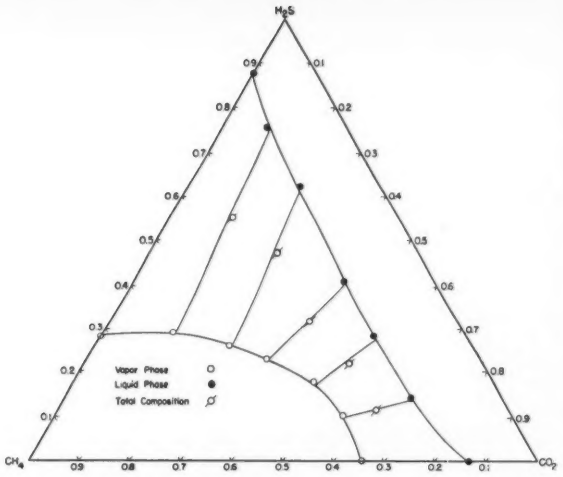

Figure 2—Phase diagram at 40°F. and 1000 lb./in.² abs.

extends from the methane-hydrogen sulphide axis to the carbon dioxide-hydrogen sulphide axis. In Figure 2, the system pressure is between the vapor pressure of carbon dioxide and the critical pressure of the methane-carbon dioxide pair and so the two phase region extends from the methane-hydrogen sulphide axis to the methane-carbon dioxide axis. Figure 3 illustrates the case where the system pressure is above the criticial pressure of the methane-carbon dioxide system but below the critical pressure of the methane-hydrogen sulphide system; and, as a result, the two phase region has diminished to a small area along the methane-hydrogen sulphide axis.

A similar shifting of the three component two phase region occurs with increase in system pressure at a temperature of 160°F. However, the two phase region never extends to the methane-carbon dioxide axis as vapor-liquid equilibrium cannot occur in the binary system methane-carbon dioxide at 160°F.

Equilibrium Ratios

Calculated equilibrium ratios are presented in Table 2 and the effects of total pressure and system composition upon the equilibrium ratio are illustrated graphically for a temperature of 160°F. by Figures 4, 5, and 6. The vapor and liquid compositions reported in this table are based on a smooth curve passing through the experimental points. Equilibrium ratios were calculated at regular intervals of an arbitrary composition parameter, C, introduced to permit comparison of experimental values taken for random system compositions at each of the pressures studied. Values of zero and unity represent the binary systems methane-hydrogen sulphide and carbon dioxide-hydrogen sulphide respectively. The curves for the binary systems were used as guides in drawing curves through the experimental data for the ternary system. Equilibrium ratios for methane do not occur, at any pressure, for a parameter of unity since this corresponds

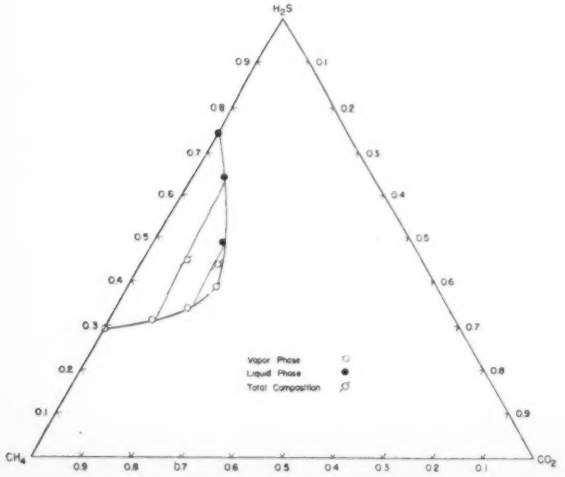

Figure 3—Phase diagram at 40°F. and 1600 lb./in.² abs.

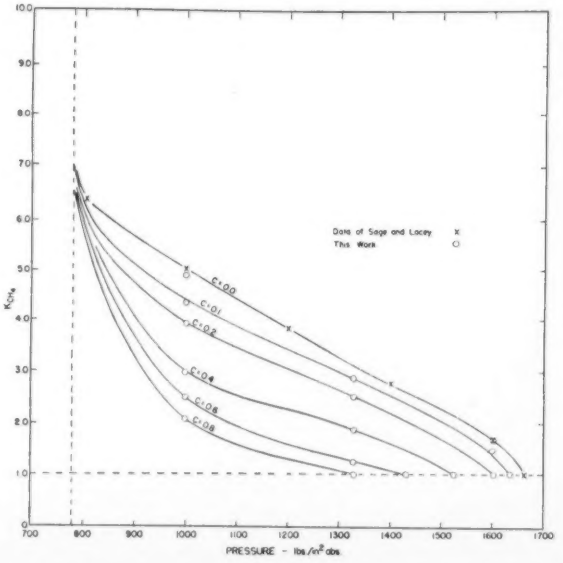

Figure 4—Equilibrium ratios for methane at 160°F.

TABLE 2

CALCULATED EQUILIBRIUM RATIOS AND ACTIVITY COEFFICIENT RATIOS

C	Vapor Composition (mole fraction)			Liquid Composition (mole fraction)			Equilibrium Ratio			Activity Coefficient Ratio		
	H_2S	CO_2	CH_4	H_2S	CO_2	CH_4	H_2S	CO_2	CH_4	H_2S	CO_2	CH_4
	Temperature = 40°F.						Pressure = 400 lbs/in.² abs.					
0.0	0.493	0.0	0.507	0.966	0.0	0.034	0.510	–	14.9	1.11	–	2.08
0.1	0.482	0.052	0.466	0.960	0.004	0.036	0.503	13.0	13.0	1.15	10.1	1.89
0.2	0.471	0.106	0.423	0.944	0.020	0.036	0.498	5.30	11.8	1.18	4.11	1.72
0.4	0.450	0.220	0.330	0.866	0.098	0.036	0.520	2.25	9.15	1.24	1.82	1.35
0.6	0.426	0.344	0.230	0.763	0.204	0.033	0.558	1.69	6.97	1.28	1.36	1.07
0.8	0.402	0.478	0.120	0.675	0.307	0.018	0.596	1.56	6.67	1.30	1.28	0.903
1.0	0.372	0.628	0.0	0.601	0.399	0.0	0.619	1.57	–	1.33	1.24	–
	Temperature = 40°F.						Pressure = 1000 lbs/in.² abs.					
0.0	0.284	0.0	0.716	0.878	0.0	0.122	0.324	–	5.87	1.10	–	1.90
0.1	0.290	0.071	0.639	0.821	0.041	0.138	0.353	1.73	4.63	1.21	2.30	1.57
0.2	0.292	0.142	0.566	0.752	0.098	0.150	0.388	1.45	3.77	1.35	1.91	1.31
0.4	0.249	0.301	0.450	0.567	0.270	0.163	0.439	1.12	2.76	1.52	1.45	0.902
0.6	0.150	0.510	0.340	0.231	0.590	0.179	0.649	0.864	1.90	2.21	1.13	0.623
	Temperature = 40°F.						Pressure = 1600 lbs/in.² abs.					
0.0	0.292	0.0	0.708	0.744	0.0	0.256	0.393	–	2.77	1.54	–	1.21
0.1	0.305	0.069	0.626	0.663	0.051	0.286	0.460	1.35	2.19	1.77	2.02	0.905
0.2	0.331	0.134	0.535	0.547	0.114	0.339	0.605	1.18	1.58	2.35	1.79	0.690
0.286	0.388	0.175	0.437	0.388	0.175	0.437	1.00	1.00	1.00	3.84	1.49	0.476
	Temperature = 160°F.						Pressure = 1000 lbs/in.² abs.					
0.0	0.844	0.0	0.156	0.968	0.0	0.032	0.872	–	4.87	1.04	–	0.550
0.1	0.840	0.0165	0.138	0.961	0.006	0.033	0.785	2.75	4.18	1.05	1.67	0.465
0.2	0.837	0.033	0.130	0.953	0.013	0.034	0.879	2.40	3.82	1.05	1.54	0.421
0.4	0.830	0.068	0.101	0.935	0.031	0.034	0.888	2.19	2.97	1.05	1.33	0.325
0.6	0.823	0.106	0.0705	0.916	0.056	0.028	0.898	1.90	2.52	1.07	1.15	0.275
0.8	0.816	0.148	0.036	0.899	0.085	0.017	0.908	1.74	2.12	1.07	1.05	0.232
1.0	0.811	0.189	0.0	0.891	0.109	0.0	0.910	1.73	0.00	1.08	1.05	–
	Temperature = 160°F.						Pressure = 1330 lbs/in.² abs.					
0.0	0.730	–	0.270	0.915	–	0.085	0.800	–	3.25	1.06	–	0.46
0.1	0.728	0.028	0.244	0.900	0.012	0.088	0.809	2.33	2.77	1.07	1.57	0.39
0.2	0.724	0.056	0.220	0.885	0.026	0.089	0.817	2.15	2.47	1.08	1.45	0.35
0.3	0.719	0.083	0.198	0.871	0.042	0.087	0.825	1.96	2.27	1.09	1.32	0.32
0.4	0.709	0.116	0.175	0.839	0.066	0.095	0.845	1.75	1.85	1.11	1.18	0.26
0.5	0.700	0.150	0.150	0.800	0.100	0.100	0.875	1.50	1.50	1.15	1.01	0.21
0.6	0.689	0.186	0.125	0.761	0.139	0.100	0.905	1.34	1.25	1.20	0.91	0.18
0.7	0.675	0.225	0.100	0.718	0.197	0.085	0.940	1.24	1.18	1.24	0.84	0.17
	Temperature = 160°F.						Pressure = 1600 lbs/in.² abs.					
0.0	0.735	0.0	0.265	0.841	0.0	0.159	0.873	–	1.67	1.25	–	0.281
0.1	0.735	0.027	0.238	0.821	0.019	0.160	0.895	1.42	1.49	1.28	1.19	0.235
0.20	0.745	0.049	0.205	0.785	0.044	0.171	0.950	1.11	1.20	1.35	0.933	0.202
0.22	0.755	0.051	0.194	0.755	0.051	0.194	1.00	1.00	1.00	1.43	0.840	0.168

to a system which does not contain any methane. Similarly, no equilibrium ratios for carbon dioxide exist for a parameter of zero.

The equilibrium ratio must have a value of unity at the critical pressure and temperature corresponding to each particular system composition. This is illustrated in Figures 4, 5, and 6 which show the equilibrium ratio versus pressure curves terminating at a value of unity for each value of the composition parameter. The critical pressure for each system was obtained from a plot of C versus critical pressure at each temperature. At 40°F. this curve was drawn through the published critical pressure for the methane-hydrogen sulphide system, the experimental ternary critical composition at 1600 lb./in.² abs., and an estimated critical pressure and composition for the methane-carbon dioxide system, based upon published data for a temperature of 29°F. [4]. At 160°F., the curve was drawn through the published critical pressure for the methane-hydrogen sulphide system, the experimental ternary critical composition at 1330 and 1600 lb./in.² abs., and the published critical pressure for the carbon dioxide-hydrogen sulphide system.

Activity Coefficient Ratios

Activity coefficient ratios were calculated at regular intrevals of the composition parameter from smoothed experimental equilibrium ratio data. The required theoretical equilibrium ratios, $\frac{f_L^*}{f_V}$, were computed from the

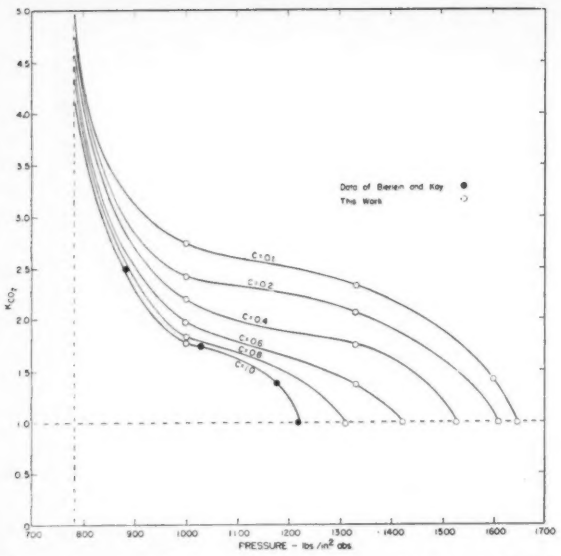

Figure 5—Equilibrium ratios for carbon dioxide at 160°F.

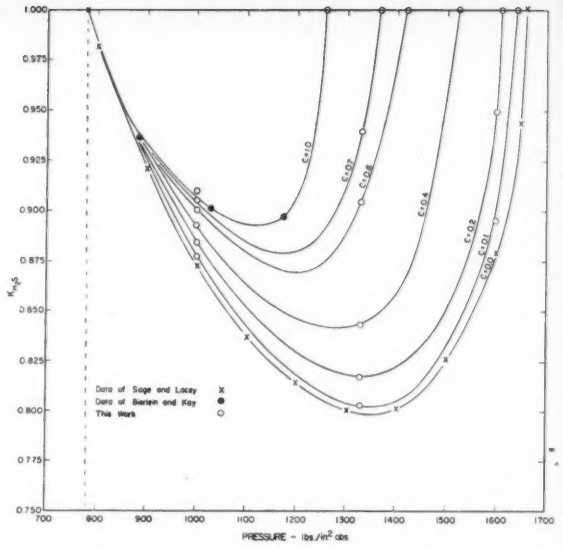

Figure 6—Equilibrium ratios for hydrogen sulphide at 160°F.

properties of the pure components using the technique discussed in Part I of this study.

The critical temperature of methane is below the system temperature at both 40°F. and 160°F., and hence the vapor pressure of pure methane at the system temperature is imaginary. By extrapolation of known vapor pressure data, values of 4100 and 9300 lb./in.² abs. were obtained for temperatures of 40°F. and 160°F. respectively. Pressure-volume data for methane at 160°F. were obtained directly from the literature [6] while those for 40°F. were obtained by interpolation of published values for temperatures of 32°F. [5], 70°F. [6] and 100°F. [6].

Carbon dioxide has a critical temperature which is below 160°F. but above 40°F. At the higher temperature a value of 2350 lb./in.² abs. for the vapor pressure was obtained by extrapolation of known values and pressure-volume data were obtained by interpolation of published data [7]. At the lower temperature, pressure-volume data for pressures below the vapor pressure were obtained by interpolation of published values at 0°F. and 50°F. [7].

Both temperatures of the investigation were below the critical temperature of hydrogen sulphide and hence vapor pressure data were available. Pressure-volume data, up to the vapor pressure, were obtained directly from the literature for temperatures of 40°F. and 160°F. [9].

Calculated activity coefficient ratios, at regular intervals of the composition parameter, are presented in Table 2 and the effect of pressure and system composition is illustrated for hydrogen sulphide at 40°F. by Figure 7 and for carbon dioxide at 160° by Figure 8. The activity coefficient versus composition parameter curves are terminated at the maximum value of the composition parameter corresponding to a system in which vapor-liquid equilibrium occurs at the conditions of pressure and temperature specified. The calculations indicate that for all three components the volatility is decreased, relative to that predicted by ideal solution laws, by an increase in temperature. However, an increase in pressure decreases the volatility of the more volatile components and increases the volatility of the less volatile component.

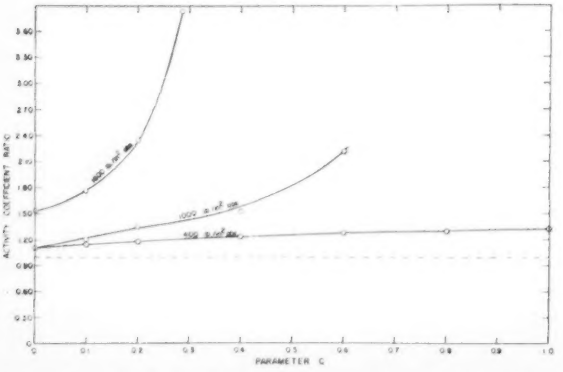

Figure 7—Activity coefficient ratios for hydrogen sulphide at 40°F.

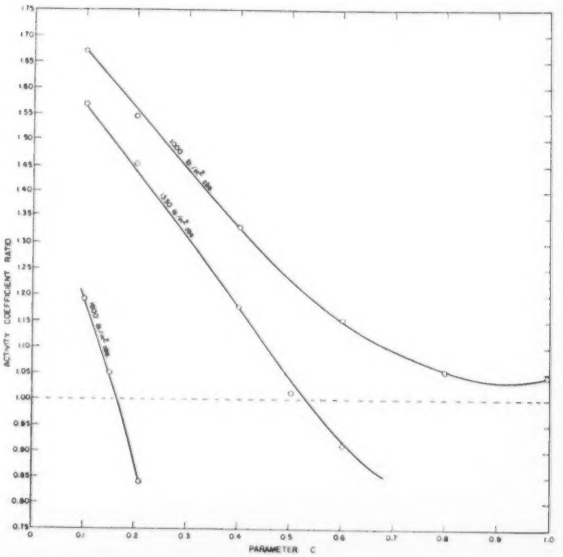

Figure 8—Activity coefficient ratios for carbon dioxide at 160°F.

Conclusions

At 40°F., the hydrogen sulphide-carbon dioxide-methane system forms co-existing vapor and liquid phases over a pressure range from 160 lb./in.^{2} abs., the vapor pressure of hydrogen sulphide, to 1949 lb./in.^{2} abs., the critical pressure of the methane-hydrogen sulphide system. Systems having a wide range of compositions form two phases between these two pressure extremes. At 160°F., the pressure range over which vapor-liquid equilibrium occurs is more limited, extending from 779 lb./in.^{2} abs. to 1660 lb./in.^{2} abs., and the overall system must be rich in hydrogen sulphide in all cases. A locus of ternary critical points exists at 40°F. from the binary critical point for the methane-carbon dioxide system, at approximately 1240 lb./in.^{2} abs. to the binary critical point for the methane-hydrogen sulphide system at 1949 lb./in.^{2} abs. At 160°F., the locus of ternary critical points extends from the binary critical point for the carbon dioxide-hydrogen sulphide system at 1220 lb./in.^{2} abs., to the binary critical point for the methane-hydrogen sulphide system at 1660 lb./in.^{2} abs.

Acknowledgment

The financial support provided by the National Research Council of Canada is gratefully acknowledged.

Nomenclature

C = composition parameter defined as the ratio of the mole fraction of carbon dioxide in the vapor phase to the sum of the mole fractions of methane and carbon dioxide in the vapor phase, dimensionless.
f_L^* = fugacity of a pure component at a pressure equal to its own vapor pressure at the system temperature, atm.
f_v = fugacity of a pure component as a vapor at the pressure and temperature of the system, atm.
K_i = equilibrium ratio for component i, dimensionless.
x_i = mole fraction of component i in the liquid phase, dimen sionless.
y_i = mole fraction of component i in the vapor phase, dimen sionless.
γ_i = activity coefficient ratio for component i, dimensionless.

References

(1) Robinson, D. B., and Bailey, J. A., C.J. Ch. E., **34**, 151 (1957).
(2) Reamer, H. H., Sage, B. H., and Lacey, W. N., Ind. Eng. Chem., **43**: 976 (1951).
(3) Bierlein, J. A., and Kay, W. B., Ind. Eng. Chem., **45**, 618 (1953).
(4) Donnelly, H. G., and Katz, D. L., Ind. Eng. Chem., **46**, 511 (1954).
(5) Perry, J. H., "Chemical Engineers' Handbook", McGraw-Hill Book Co., Inc., New York (1950).
(6) Olds, R. H., Reamer, H. H., Sage, B. H., and Lacey, W. N., Ind. Eng. Chem., **35**, 922 (1943).
(7) Sweigert, R. L., Weger, P., and Allen, R. L., Ind. Eng. Chem., **38**, 185 (1946).
(8) Hougen, O. A., and Watson, R. M., "Chemical Process Principles", Part II, John Wiley and Sons Inc., New York (1947).
(9) Reamer, H. H., and Sage, B. H., Ind. Eng. Chem., **42**, 140 (1950).

★ ★ ★

Liquid-Liquid Extraction with Association Effects[1]

J. D. RAAL[2] and A. I. JOHNSON[3]

A special case of liquid-liquid extraction as been considered where the solute on absorption reacts to form a dimer through a rapid second order reversible reaction with the solvent.

If dimer and monomer have different diffusivities (in the same solvent) the rate of absorption becomes dependent on the ratio of these diffusivities and the isotherm governing the "association" reaction.

The non linear differential equation governing the absorption was solved numerically with the aid of a digital computer for the case of resistance in one phase only.

Correlations based on these solutions were then used in formulating a rate equation. Methods were suggested for the determination of the quantities occurring in the "driving force" of the predicted rate equation.

In liquid-liquid extraction, interphase mass transfer rates have been represented generally by the rate equation

$$N = K_m A(c^* - c) \quad \ldots\ldots(1)$$

where K_m is a mass transfer coefficient, A_i is the interfacial area, and $(c^* - c)$ is an over-all driving force. In the driving force c^* represents the concentration in the raffinate phase, from which solute is transferring, as an equivalent or "equilibrium" concentration in extract phase concentration units.

If one considers transfer between two stirred liquids with a known interfacial area in an apparatus such as that used by Lewis [1] or by Gordon and Sherwood [2] the transfer rate is equal to the rate of accumulation in the extract phase

$$N = V\left(\frac{dc}{dt}\right) \quad \ldots\ldots(1a)$$

where V is the volume of the extract phase.

From (1) and (1a) it is apparent that the mass transfer coefficient K_m could be calculated from the slope of a graph of $\int \frac{V\,dc}{c^* - c}$ against time t.

A typical plot of such data is shown as Figure 1 for the batchwise extraction of propionic acid from water into isopropyl ether. Since the integration accounts for change in volume during the transfer process, the marked curvature of the plot indicates that perhaps the simple driving force $(c^* - c)$ used in (1) is not correct. It should be noted that for the system of Figure 1 the distribution coefficient was constant over the range of concentrations of the figure.

It is well known [3, 4, 5] that when organic acids or amides are transferred between water and an organic solvent there will be molecular associations in the organic phase and dissociations in the aqueous phase. It is the purpose of this paper to examine how such effects may require modification of the driving force for the mass transfer of such solutes at an interface such as is sketched in Figure 2.

Theoretical Considerations

Formulation of the controlling partial differential equation

Considering a solute, HA, diffusing in an organic phase it will be assumed that there is an instantaneous equilibrium between the monomer and dimer at any point:

$$2HA \rightleftharpoons (HA)_2 \quad \ldots\ldots(2)$$

The molecules will diffuse according to Fick's law:

$$N_{c_1} = -D_1\left(\frac{\partial c_1}{\partial x}\right) \quad \ldots\ldots(3a)$$

$$N_s = -D_2\left(\frac{\partial s}{\partial x}\right) \quad \ldots\ldots(3b)$$

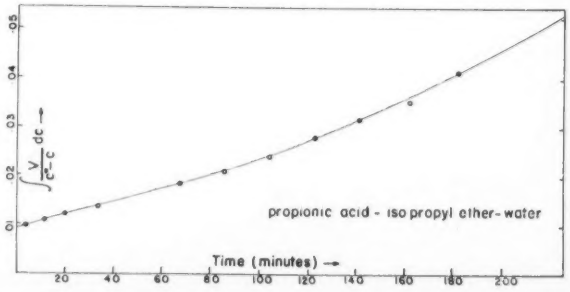

Figure 1—Test of driving force $(c^* - c)$. (Volume variation taken into account).

[1]*Manuscript received June 30, 1959.*
[2]*Graduate Student, Department of Chemical Engineering, University of Toronto, Toronto, Ont.*
[3]*Associate Professor, Department of Chemical Engineering, University of Toronto, Toronto, Ontario.*
Contribution from the Department of Chemical Engineering, University of Toronto, Toronto, Ont.

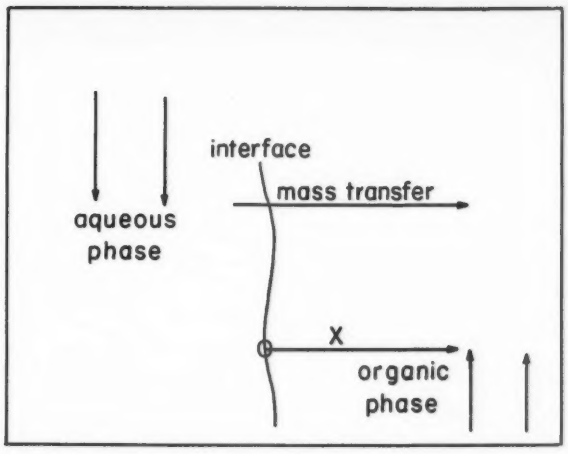

Figure 2—Schematic representation of interface.

where D_1 and D_2 are the diffusivities and c_1 and s are the point concentrations of monomer and dimer respectively.

The forms of Fick's second law, obtained in the normal manner, are

$$D_1 \frac{\partial^2 c_1}{\partial x^2} = \frac{\partial c_1}{\partial t} + \gamma \quad \ldots\ldots (4a)$$

$$D_2 \frac{\partial^2 s}{\partial x^2} = \frac{\partial s}{\partial t} - 1/2\gamma \quad \ldots\ldots (4b)$$

where γ = rate of association, moles HA/litre)(sec.).

Here γ represents a fast but finite production of dimer and should not be confused with rate constants that may be associated with Equation (2).

Corresponding to the semi-instantaneous equilibrium described by Equation (2) the equilibrium constant K_e is defined by:

$$s = K_e c_1^2 \quad \ldots\ldots (5)$$

Using γ from (4b) and s from (5) permits (4a) to be written as

$$\frac{1}{D_2}\left(\frac{\partial c_1}{\partial t}\right) = \frac{r}{\frac{1}{4K_e} + c_1}\left(\frac{\partial^2 c_1}{\partial x^2}\right) + \frac{1}{\frac{1}{4K_e} + c_1}\left(\frac{\partial c_1}{\partial x}\right)^2 \quad \ldots\ldots (6)$$

where

$$r = D_1/D_2 \quad \ldots\ldots (6a)$$

It should be pointed out that if the analytical concentration is used

$$\phi = c_1 + 2s \quad \ldots\ldots (7a)$$

and if we define

$$D_e = D_1 - 2(D_1 - D_2)\left(\frac{\partial s}{\partial x}\right) \quad \ldots\ldots (7b)$$

then Equation (6) would revert to the ordinary form of Fick's second law

$$\frac{\partial \phi}{\partial t} = \frac{\partial}{x}\left(D_e \frac{\partial \phi}{\partial x}\right) \quad \ldots\ldots (8)$$

and if the diffusivities of monomer and dimer were equal there would be no difficulty in analysing the diffusion of an associated solute.

Although the solution of Equation (8) with variable D_e values has been treated extensively by Crank [6] and others [7, 8, 9], the present authors have not found Equation (6) solved in the literature.

Solution of the partial differential equation

We shall consider only the simplest transfer situation as illustrated in Figure 2, that is, transfer into essentially an infinite extent of organic phase from an interface at which there is a constant equilibrium value c_1^*. If the initial uniform concentration is c_1° and if one defines

$$a = \frac{1}{4K_e c_1^*} \quad \ldots\ldots (9a)$$

and

$$C = \frac{c_1}{c_1^*} \quad \ldots\ldots (9b)$$

$$C^\circ = \frac{c_1^\circ}{c_1^*} \quad \ldots\ldots (9c)$$

then Equation (6) becomes

$$\frac{1}{D_2}\left(\frac{\partial C}{\partial t}\right) = \frac{C + ar}{C + a}\left(\frac{\partial^2 C}{\partial x^2}\right) + \frac{1}{C + a}\left(\frac{\partial C}{\partial x}\right)^2 \quad \ldots\ldots (10)$$

to be solved for the boundary conditions

$$x = 0, \quad t > 0, \quad C = 1 \quad \ldots\ldots (11a)$$

$$x = \infty, \quad t \geq 0, \quad C = C^\circ \quad \ldots\ldots (11b)$$

$$x > 0, \quad t = 0, \quad C = C^\circ \quad \ldots\ldots (11c)$$

Utilization of the Boltzman transformation (6):

$$y = \frac{x}{2\sqrt{D_2 t}} \quad \ldots\ldots (12)$$

converts (10) to the ordinary differential equation

$$-2y\left(\frac{dC}{dy}\right) = \frac{C + ar}{C + a}\left(\frac{d^2 C}{dy^2}\right) + \frac{1}{C + a}\left(\frac{dC}{dy}\right)^2 \quad \ldots\ldots (13)$$

and the boundary conditions (11) to

$$y = 0, \quad C = 1 \quad \ldots\ldots (14a)$$

$$y = \infty, \quad C = 0 \text{ (for the case where } C^\circ = 0) \quad \ldots\ldots (14b)$$

In a trial solution of (13) on the Beckman EASE analogue computer, initial values of C and $\left(\frac{dC}{dy}\right)$ were selected (the latter arbitrarily) for the computation. Solutions satisfying the second boundary condition (14b) could not be obtained, however.

This may have been due to the introduction of the squared relationship $s = K_e c_1^2$ into the differential equation which provided the possibility of having negative as well as positive values c_1 which satisfy the differential equation and initial conditions.

A numerical solution was found as outlined below, incorporating the boundary condition

$$y = \infty, \quad C = \frac{dC}{dy} = 0 \quad \ldots\ldots (15)$$

(since there is zero flux at zero concentration), in a manner superficially similar to that used by Wagner [9].

Corresponding to some very small arbitrary value $C = \delta$, there exists a value of $y = y_o$. By the transformations

$$m = 1 - \frac{y}{y_o} \quad \ldots\ldots (16a)$$

$$P = \frac{C - \delta}{y_o^2} \quad \ldots\ldots (16b)$$

Equation (13) becomes

$$\frac{d^2P}{dm^2} = 2y_o(1 - m)\frac{P + k_2}{P + k_1}\left(\frac{dP}{dm}\right) - \frac{1}{P + k_1}\left(\frac{dP}{dm}\right)^2 \quad \ldots(17)$$

where

$$k_1 = \frac{ar + \delta}{y_o^2} \quad \ldots(18a)$$

$$k_2 = \frac{a + \delta}{y_o^2} \quad \ldots(18b)$$

Equation (17) can be simplified even further by the transformation

$$\sqrt{z} = C + ar \quad \ldots(19)$$

to give

$$\frac{\sqrt{z}}{\sqrt{z} + a - ar}\left(\frac{d^2z}{dy^2}\right) = -2y\left(\frac{dz}{dy}\right) \quad \ldots(20)$$

For $y = y_o$ on the right side, (20) can be integrated to yield

$$\frac{dz}{dy} = -2y_o\{z + 2a(1 - r)\sqrt{z}\} + \text{a constant} \quad \ldots(21)$$

By having δ sufficiently small that (15) holds, it can be shown that the integration constant of (21) is zero. It follows finally from (21) that

$$\left(\frac{dP}{dm}\right)_{m=o} = \frac{\delta(2a + \delta)}{ar + \delta} \simeq \frac{2\delta}{r} \quad \ldots(22)$$

This latter equation provides an initial slope for the solution of Equation (17) by the Runge Kutta equations as modified by Gill [10]. To do this the following steps were taken using an IBM 650 computer:

(a) A value of δ of the order of 10^{-5} was fixed arbitrarily.

(b) A suitable value of y_o was assumed. As a first approximation the value obtained for diffusion of a simple molecule for $C = \delta = 10^{-5}$ may be used.

(c) The values of $\left(\frac{dP}{dm}\right)_{m=o}$, k_1 and k_2 were obtained using (22) and (18).

(d) The curve of P against m was computed from $m = o$ to $m = 1$.

(e) The value of P at $m = 1$ was compared with $\frac{1 - \delta}{y_o^2}$; if no agreement was found a new assumption of y_o was necessary.

Typical computation results

Figure 3 shows typical curves obtained by the above procedure for the a and r values shown. In Figure 4 these are converted to the more useful curves of C against y and are compared with the curve for diffusion of a simple molecule of diffusivity D_1.

The areas under the curves of Figure 4 also provide values of the total amount of solute that has diffused to any time t. This can be compared with the amount that has crossed the interface until this time.

Thus, total moles absorbed =

$$W_t = \int_o^\infty (c_1 + 2s)dx = \int_o^t -\left\{D_1\left(\frac{\partial c_1}{\partial x}\right)_{x=o} + 2D_2\left(\frac{\partial s}{\partial x}\right)_{x=o}\right\}dt \quad \ldots(23)$$

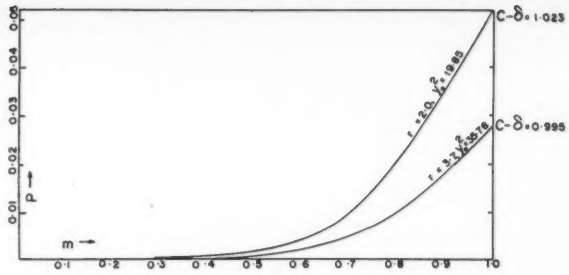

Figure 3—Numerical solution of differential equation for a = 0.7.

From Equation (23) we find:

$$-\left(\frac{dc}{dy}\right)_{y=o} = \frac{2a}{ar + 1}\left\{\int_o^\infty Cdy + \frac{1}{2a}\int_o^\infty C^2dy\right\} \quad \ldots(24)$$

Equation (24) may be used as a check on the internal consistency of the numerical solutions obtained.

In the preceding derivation the flux at the interface was written as

$$-D_1\left(\frac{\partial c_1}{\partial x}\right)_{x=o} - 2D_2\left(\frac{\partial s}{\partial x}\right)_{x=o},$$

whereas it is probable that only unassociated molecules as such cross the interface. One could reason that physically the equilibrium between dimer and monomer assumed in this paper exists up to the immediate neighbourhood of the interface. In the derivation of the differential equation the isotherm $s = K_e c_1^2$ was assumed to hold for all x including $x = o$, and the flux $-2D_2\left(\frac{\partial s}{\partial x}\right)$ must therefore be included in Equation (23).

In Table 1 are shown typical results obtained from the application of the area test discussed previously.

Transfer rates at an interface

Let us now see how the above computations can be applied to transfer rates at an interface.

For $r = 1$, the differential Equation (13) may be solved formally by noting that the substitutions $\sqrt{z} = (C + ar)$; $\frac{dz}{dy} = Q$, will reduce the equation to a form in which the variables may be separated. The solution is:

$$-\left(\frac{dC}{dy}\right)_{y=o} = \frac{1}{\sqrt{\pi}}\left(\frac{a}{a + 1}\right) + \frac{1}{\sqrt{\pi}} \quad \ldots(25)$$

TABLE 1
"AREA" TEST

a	r	$-\left(\frac{dC}{dy}\right)_{y=o}$	$\frac{2a}{ar + 1}\left\{\int_o^\infty Cdy + \frac{1}{2a}\int_o^\infty C^2dy\right\}$
0.15	2.0	.602	.600
0.25	2.0	.627	.635
0.30	2.0	.644	.648
0.70	3.7	.578	.581

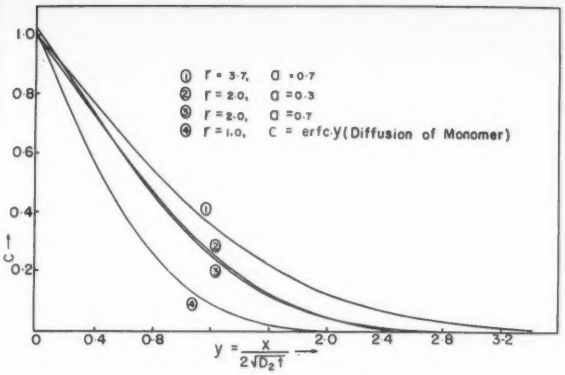

Figure 4—Numerical solution of differential equation.

For other r values the following empirical correlation was found to fit well

$$-\left(\frac{dC}{dy}\right)_{y=o} = b'\left(\frac{ar}{ar+1}\right) + \frac{1}{\sqrt{\pi}} \quad \ldots\ldots(26)$$

where

$$b' = \frac{1}{\sqrt{\pi}}\left(\frac{2}{r+1}\right)^r \quad \ldots\ldots(26a)$$

Figure 5 shows a plot of the above correlation and Table 2 shows the correlation of b′ for Equation (26a).

The transfer rate at the interface

$$R(t) = -D_1\left(\frac{\partial c_1}{\partial x}\right)_{x=o} - 2D_2\left(\frac{\partial s}{\partial x}\right)_{x=o} \quad \ldots\ldots(27)$$

$$= -\frac{1}{8K_e}\sqrt{\frac{D_1}{rt}}\left(\frac{ar+1}{a^2r}\right)\left(\frac{dC}{dy}\right)_{y=o} \quad \ldots\ldots(27a)$$

Using (26) where $b = \sqrt{\pi}\,b'$, this rate expression becomes

$$R(t) = \frac{1}{8K_e}\sqrt{\frac{D_2}{\pi t}}\left\{\frac{b}{a} + \frac{ar+1}{a^2r}\right\} \quad \ldots\ldots(28)$$

If now analytical concentrations be used, then (28) can be written as

$$R(t) = \frac{1}{8K_e}\sqrt{\frac{D_2}{\pi t}}\,(p^* - 1)\left\{p^* + b + (r-1)(b+1)\right\} \quad \ldots(29)$$

where

$$p^* = \sqrt{1 + 8K_e\phi^*} \quad (30a)$$

and

$$\phi^* = c_1^* + 2s^* \quad \ldots\ldots(30b)$$

TABLE 2

r	b	$\left(\frac{2}{r+1}\right)^r$
1.0	1.0	1.0
2.0	0.422	0.444
3.7	0.042	0.042

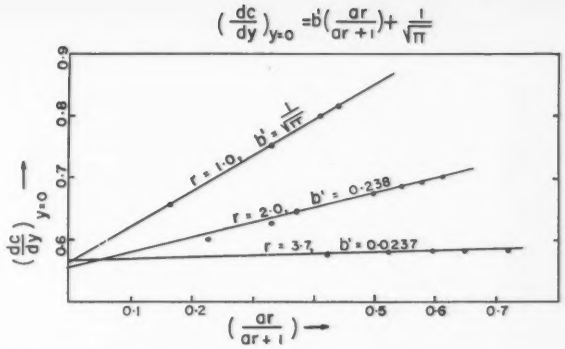

Figure 5—Initial slope correlation.

For the more general case where $C^\circ \neq o$, the rate equation corresponding to (29) is

$$R(t) = \frac{1}{8K_e}\sqrt{\frac{D_2}{\pi t}}\,(p^* - p^\circ)\left\{p^* + Bp^\circ + (r-1)(B+1)\right\} \quad \ldots(31)$$

where

$$B = \left(\frac{2}{R+1}\right)^R \quad \ldots\ldots(32a)$$

$$p^\circ = \sqrt{1 + 8K_e\phi^\circ} \quad \ldots\ldots(32b)$$

and

$$R = \frac{4K_ec_1^\circ + r}{4K_ec_1^\circ + 1} = 1 + \frac{r-1}{p^\circ} \quad \ldots\ldots(32c)$$

The average rate of absorption for a short period of exposure (t_e) can now be written down using either the Higbie [11] or Danckwerts [12] method.

$$R_{ave} = \frac{1}{t_e}\int_o^{te} R(t)dt = \frac{1}{4K_e}\sqrt{\frac{D_2}{\pi t_e}}\,(p^* - p^\circ) \times$$

$$\left\{p^* + Bp^\circ + (r-1)(B+1)\right\} =$$

$$K_m(p^* - p^\circ)\left\{p^* + Bp^\circ + (r-1)(B+1)\right\} \text{ (Higbie)} \quad \ldots(33)$$

or

$$R_{ave} = s'\int_o^{\infty} e^{-s't}R(t)dt = \frac{\sqrt{D_2 s'}}{8K_e}\,(p^* - p^\circ) \times$$

$$\left\{p^* + Bp^\circ + (r-1)(B+1)\right\} =$$

$$K_m'(p^* - p^\circ)\left\{p^* + Bp^\circ + (r-1)(B+1)\right\} \text{ (Danckwerts)} \quad (33a)$$

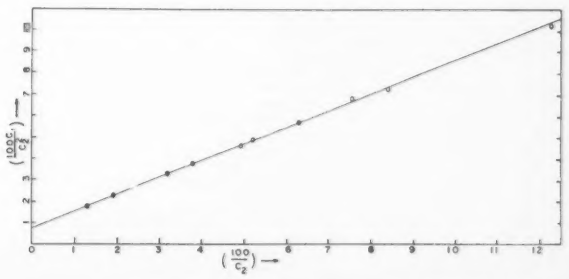

Figure 6—Distribution plot: propionic acid-isopropyl ether-water (25°C.).

Determination of K_e and r

In order to evaluate the "driving force" $(p^* - p^\circ)\{p^* + Bp^\circ + (r-1)(B+1)\}$, it is necessary to determine the quantities K_e and r with some accuracy.

Determination of K_e: The equilibrium constant may be determined from distribution data in a simple manner: Consider the distribution of the acid HA between water (phase II) and a suitable organic liquid (phase I). If a linear distribution relationship exists between *like* species of acid in the two phases (e.g. between simple HA molecules, neither associated nor dissociated) this may be written as

$$c_{II} = M'c_I = 4K_eMc_I \quad \ldots\ldots (34)$$

where M_1 and M are distribution coefficients defined by this equation. In the organic phase

$$2HA \rightleftharpoons (HA)_2$$
$$(c_I) \qquad (s)$$

Analytical concentration

$$\phi_I = c_I + 2s = c_I + 2K_ec_I^2$$

$$\therefore 4K_ec_I = \sqrt{1 + 8K_e\phi_I} - 1 \quad \ldots\ldots (35)$$

Hence the distribution relationship becomes

$$c_{II} = M\{\sqrt{1 + 8K_e\phi_I} - 1\} \quad \ldots\ldots (36)$$

For weak acids (36) may be arranged in the form

$$\frac{\phi_I}{\phi_{II}^2} = \frac{1}{M'}\left(\frac{1}{\phi_{II}}\right) + \frac{2K_e}{(M')^2} \quad \ldots\ldots (36a)$$

This equation in slightly different form, was proposed by Davies [13] et al. These authors found their equation to predict satisfactorily the distribution of acetic and propionic acids between water and a number of organic solvents in concentrations up to 1N.

Thus if $\frac{\phi_I}{\phi_{II}^2}$ be plotted against $\frac{1}{\phi_{II}}$, K_e (and M') may be found from the intercept and slope if the plot is linear. In Figure 6 is shown the distribution data for the system propionic acid-isopropyl ether-water plotted according to Equation (36a).

Association constants obtained in this manner should be accepted with caution, however. Lassettre [5] has pointed out that hydration in the organic phase may lead to erroneous conclusions regarding equilibrium constants if this effect is not taken into account.

Determination of r and D_2: It has been pointed out previously (cf. Equation (7b)), that the diffusion model predicts a concentration-dependent diffusion coefficient in terms of analytical concentration, for the organic phase. The "effective" diffusion coefficient De was shown to be

$$D_e = D_1 - 2(D_1 - D_2)\left(\frac{\partial s}{\partial \phi}\right),$$

or in terms of ϕ,

$$D_e = D_2 + \frac{D_2(r-1)}{\sqrt{1 + 8K_e\phi}} \quad \ldots\ldots (37)$$

Thus, if the differential diffusion coefficient D_e is plotted against concentration the model predicts a curve of the form shown in Figure 7.

The values of D_1 and D_2 are then given by the intercept at infinite dilution (D_1), and the steady value at high concentration respectively. If accurate values for De can be determined at very low concentrations a value for K_e may be found by noting that

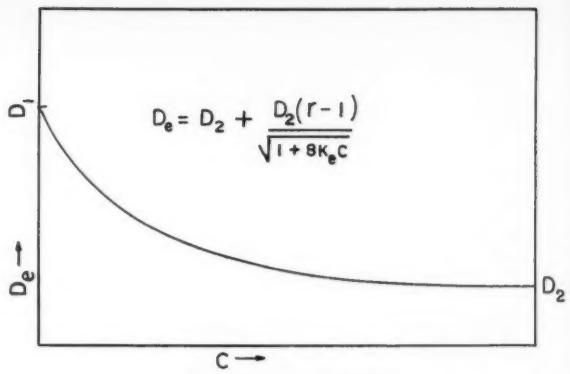

Figure 7—Predicted diffusion curve.

$$\left(\frac{dD_e}{d\phi}\right)_{\phi=0} = -4K_e(D_1 - D_2)$$

In an experimental study of the diffusion of Pamelia oil in acetone by Kaneko et al [14], the authors reported a curve corresponding to that shown in Figure 7. A rough computation (by us) from their curve gave a value for r of the order of 3.7. These authors stated: "The fact that there is no definite relationship between D and C seems to indicate that the diffusion of associated molecules is analogous to homogeneous diffusion of concentration dependent system." (Here C is a concentration in gm./100 cc. of solution.)

Summary

For the absorption of a compound into an organic liquid in which it forms a dimer, a rate equation has been proposed.

On the hypothesis that associated and unassociated species have different but constant diffusivities, if these are defined as in Equations (3), a diffusion equation was derived and numerical solutions were obtained with the aid of a digital computer for the case of constant interfacial concentration equal to the saturation value, c*. The values for initial slope of the diffusion curves thus obtained were used in a correlation involving the dimensionless constants a and r (or R) for a value of the order $0.1 < a < 0.8$, and for $r = 1.0, 2.0, 3.7$. The results of this correlation were used to predict a rate equation, using either the Higbie or Danckwerts mechanism.

These equations predicted a "driving force" of unusual complexity in which the "bulk" and saturation concentrations (ϕ and ϕ^*) were combined with such quantities as K_e, r and R.

For the determination of these quantities, methods have been suggested involving distribution measurements and determination of differential diffusion coefficient as a function of concentration.

It will be seen from the final rate equations that the value of $r = \frac{D_1}{D_2}$ is of critical importance in predicting deviations from the "normal" driving force, $(c^* - c)$.

If further diffusion measurements lend support to a prediction such as Equation (37), the quantity r may assume unusual importance and it is felt that the rate equations proposed above, although derived for rather limited boundary conditions may become very useful as a starting point for correlations of absorption and extraction rates where reactions of the type discussed occur.

Nomenclature

$a = \dfrac{1}{4K_e c_1^*}$ (dimensionless)

A_i = interface area, cm²

$b = \left(\dfrac{2}{r+1}\right)^r$ (dimensionless)

$B = \left(\dfrac{2}{R+1}\right)^R$ (dimensionless)

c_1 = concentration of unassociated species, moles HA/litre

c^* = an equilibrium concentration

c_1^* = saturation concentration of unassociated species moles HA/litre

c_1° = bulk concentration of unassociated species, moles HA/litre.

$C = \dfrac{c_1}{c_1^*}$ (dimensionless)

$C^\circ = \dfrac{c_1^\circ}{c_1^*}$ (dimensionless)

ϕ = total (analytical) concentration as moles HA/litre

D_1 = diffusion coefficient for unassociated species, cm²/sec.

D_2 = diffusion coefficient for associated species, cm²/sec.

D_e = effective differential diffusion coefficient, cm²/sec.

K_e = equilibrium constant for association reaction, litres/mole

K_m = mass transfer coefficient, cm/sec.

$k_1 = \dfrac{ar + \delta}{y_o^2}$ (dimensionless)

$k_2 = \dfrac{a + \delta}{y_o^2}$ (dimensionless)

$m = (1 - y/y_o)$

M' = distribution coefficient

$p = \sqrt{1 + 8K_e\phi}$

$P = \dfrac{C - \delta}{y_o^2}$

$r = \dfrac{D_1}{D_2}$

$R = \dfrac{r + 4K_e c_1^\circ}{1 + 4K_e c_1^\circ} = 1 + \dfrac{r-1}{p^\circ}$ (dimensionless)

s' = Danckwerts surface renewal factor

s = concentration of associated species, moles $(HA)_2$/litre

t = time, secs.

W_t = moles of acid absorbed in time t

x = coordinate in direction of diffusion (cm)

y = Boltzmann variable $\dfrac{x}{2\sqrt{D_2 t}}$ (dimensionless)

y_o = value of y for which $C = \delta$

$z = (C + ar)^2$

δ = value of C at $y = y_o$

γ = rate of association, moles HA/(litres)(sec.)

References

(1) Lewis, J. B., Chem. Eng. Sci., **3**, 248 (1954).

(2) Gordon, K. F., and Sherwood, T. K., Chem. Eng. Prog. Symp. Ser. 50, No. 10, **15** (1954).

(3) Ferguson, L. N., J. Chem. Educ., **31**, 626 (1954).

(4) Klemperer, W. Cronyn, M. W., Maki, A. H., and Pimentel, G. C., J. Am. Chem. Soc., **76**, 5846 (1954).

(5) Lassettre, E. N., Chem. Revs., **20**, 259 (1937).

(6) Crank, J., The Mathematics of Diffusion (Oxford) pp. 121, 122.

(7) Eyres, N. R., Hartree, D. R., Ingham, J., Jackson, R., Sarjant, A. J., and Wagstaff, S. M., Phil. Trans. Roy. Soc. A **240** (1946) 1.

(8) Fujita, H., Text. Res. J. **22**, 757, 823 (1952).

(9) Wagner, C., J. Chem. Phys., **18**, 1229 (1950).

(10) Gill, S., Camb. Phil. Soc. Proc., **47**, 96 (1951).

(11) Higbie, R., Trans. Amer. Inst. Chem. Engrs., **31**, 365 (1935).

(12) Danckwerts, P. V., Ind. & Eng. Chem., **43**, 1460 (1951).

(13) Davies, Jones, Moelwyn-Hughes, A. E., J. Chem. Soc., 1249 (1951).

(14) Kaneko, K., Kitamura, K., and Hosokawa, Y., Nippon Kagaku Zasshi, **77**, 1023 (1956).

★ ★ ★

Fundamental Aspects of Solids-Gas Flow

Part III. Accelerated Motion of a Particle in a Fluid[1]

L. B. TOROBIN[2] and W. H. GAUVIN[2]

An analysis of the extensive literature on non-steady drag forces supports the correlation of the data by means of a total drag coefficient, which appears to be a function of the Reynolds Number and of a reduced time parameter which is related to the number of particle diameters traversed since the initiation of the motion. The added mass concept is shown to be both completely inadequate and theoretically unsound. An increase in wake turbulence resulting from Reynolds Number increases or from the occurrence of surface roughness seems to diminish the acceleration effects.

Fundamental studies of the flow fields around blunt bodies reveal the extreme complexity of the phenomena occurring during acceleration. Explanations offered for the characteristics of the non-steady drag coefficient behavior are shown to be frequently at variances with these findings.

THE flow fields around a sphere at very low Reynolds Numbers which were discussed in Part I of this series [1], and the wake phenomena described in Part II [2] applied strictly to the case of an aerodynamically-smooth spherical particle, moving in an infinite, turbulence-free fluid. Although these idealized conditions are seldom met in actual conveying systems or solids-gas contacting operations, a knowledge of the fundamental concepts underlying the ideal motion is essential for the proper understanding and evaluation of the complicating effects commonly encountered in chemical engineering practice. The rest of this series will be devoted to a detailed study of these complicating factors, concluding with the application of this information to the study of multiparticle systems. The present paper is concerned with the effects of acceleration on particulate motion.

It has been common practice to assume that the standard curve for the drag coefficient as a function of the Reynolds Number may be applied to particles undergoing accelerated or decelerated motion in a fluid. Lapple and Shepherd [3] have ignored any possible unsteady motion effects in the development of their equations for the calculation of particle trajectories, and the same consideration applies to the work of Gilbert, Davis and Altman [4] which was concerned with the relative velocity of solids entrained in linearly-accelerated combustion gases. Khudiakow [5] and Weidner [6], have also used this simplification in the analysis of their multiparticle data, and acceleration complications have not been considered in most similar papers dealing with multiparticle solids-gas flow.

Recent experimental studies in these laboratories have illustrated the inability of the standard drag coefficient curve to predict the motion of decelerating droplets in a spray dryer [7], in an atomized-suspension reactor [8] and the motion of accelerating particles in a flash-dryer [9] thus preventing the use of particulate heat and mass transfer information to provide generalized design correlations.

The discussion which follows deals first with experimental observations of particles undergoing accelerated motion together with the superficial methods used to correlate these data, and then with the limited fundamental information presently available concerning the acceleration phenomena.

V. ACCELERATED MOTION OF A PARTICLE IN A FLUID

Macroscopic Experimental Evidence

In 1826, Bessel [10] reported experiments with a spherical pendulum moving in air and in water, and he found that to account for the observed behavior by the conventional equations of motion a so-called "added mass" M_A, which was proportional to the mass of the fluid displaced by the body, would have to be added to that of the sphere. The constant of proportionality k_A was found to be 0.9 and 0.6 for the case of air and water respectively. Others working with spheres oscillating in liquids and gases [11, 12, 13, 14, 15, 16] also found this concept useful in explaining the apparent acceleration effects indicated by their data. Applied to the case of a particle in accelerated rectilinear motion through a still fluid, the equation of forces on the particle would give:

[1] *Manuscript received October 2, 1959.*

[2] *McGill University and Pulp and Paper Research Institute of Canada, Montreal, Que.*

$$F_g = (M + M_A)\dot{U}_p + R =$$
$$(M + k_A V_p \rho)\dot{U}_p + (1/2)\, C_D \rho A_p U_p^2 \quad \ldots\ldots(1)$$

where F_g is the body force due to gravity, M the particle mass, $\dot{U}_p$ and U_p the absolute particle acceleration and velocity respectively, ρ the fluid density, A_p the particle cross-sectional area, V_p the particle volume, and R and C_D the steady state fluid drag force and drag coefficient respectively—these last two terms are assumed in this analysis to be unaffected by the acceleration. The added mass concept enjoyed varying degrees of popularity but, as will be shown, it is completely inadequate since it greatly underestimates the complexity of the flow.

Equation (1) can be rewritten in a form which would make a more plausible inference as to the nature of the acceleration effect, indicating that it acts in such a manner as to change the fluid resistance from the steady state value of R to a different one R_A, which becomes a function of the acceleration. Furthermore, it is assumed that R_A can be related to the acceleration and velocity terms by the expression:

$$R_A = k_1\dot{U}_p + k_2 U_p^2 \quad \ldots\ldots(2)$$

where k_1 and k_2 are empirical coefficients, so that a balance of forces would give:

$$F_g - M\dot{U}_p = R_A = k_1\dot{U}_p + k_2 U_p^2 \quad \ldots\ldots(3)$$

A third—and possibly the best—method of accounting for the altered drag due to the acceleration is by expressing it in terms of a modified drag coefficient, C_{DA}, defined by:

$$F_g - M\dot{U}_p = R_A = (1/2)\, C_{DA} \rho A_p U_p^2 \quad \ldots\ldots(4)$$

One of the earliest studies of rectilinear motion which hinted at possible acceleration effects was reported in 1900 by Allen [17], who noted that the drag coefficients of steel spheres slowly accelerating in water were increased from 10 to 20 percent. Later Schmidt [18], in recording the movement of wax spheres in water and of balloons in air, found their accelerations to be slower than would be predicted from steady flow drag coefficients, and his results also suggested that the C_{DA} values were a function of the magnitude of the acceleration. Schmidt made the interesting observation that eddy formation at the rear of spheres undergoing acceleration would occur at lower Reynolds Numbers than would normally appear in steady motion. This would be sure to increase the form drag of the body, and would not be accounted for by the "added mass" concept.

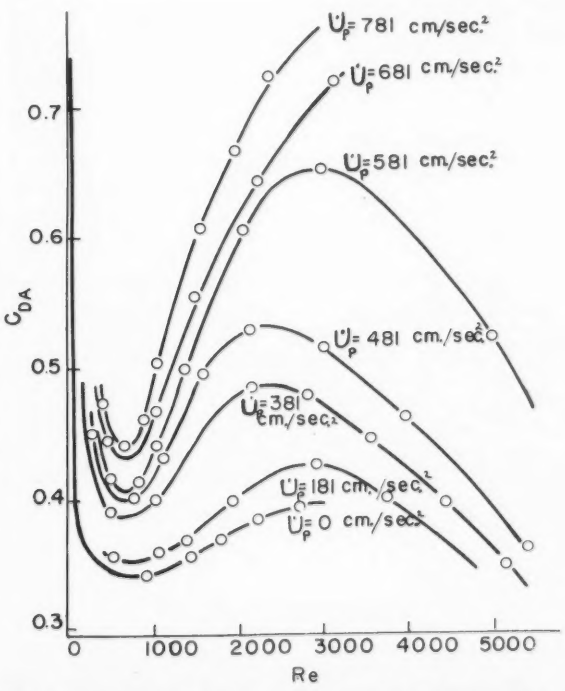

Figure 1—Drag coefficients of accelerating spheres falling in air (Lunnon).

Increased values of C_D during acceleration are also indicated by the work of Magnan and St. Lague [19] and Cook [20] for spheres moving in water, and Richardson [21], Hesselberg and Birkeland [22], Relf and Jones [23] and Hirsch [24] for spheres moving in air. Cook, Hirsch, and Relf and Jones reported added mass coefficients which varied from 0.46 to 0.83, and k_A seemed to be affected by the acceleration, the fluid density and the past history of the motion but the exact inter-relationships were obscured by experimental errors. Acceleration drag phenomena are very difficult to study since a continuous time-distance record of the particle movement is required with sufficient precision to give accurate values of the second derivative—a criterion which has rarely been attained by the investigations thus far considered.

In a series of investigations started in 1924 and which are noted for their excellence of technique, Lunnon [25, 26, 27, 28, 29, 30] studied the dynamics of spheres of varied density falling in air and in water; for the former, the precision was such that the maximum deviation between similar trials in the air was of the order of 0.002 second for distances up to 36 meters thereby furnishing usable acceleration data. Lunnon found his results to be approximated by Equation (2), although in the initial stages of motion the resistance was higher and in the final stages lower than the average resistance throughout the acceleration region. Lunnon was able to construct smooth curves through his results for air when he plotted them on co-ordinates which were directly proportional to C_{DA} and Re. The authors of this survey have replotted some of Lunnon's data in a more conventional manner, using C_{DA} and Re as the ordinate and abscissa respectively (Figure 1), and these show that even moderate accelerations can have marked effects on the drag coefficient, depending on the particle Reynolds Number regime. These experimental results may not be too general, since they were all obtained from trials in which the spheres were of equal density. Lunnon's data for water were not sufficiently accurate to be presented by such an analysis, but they indicate that C_{DA} will be affected considerably by the fluid density.

The "added mass" analysis when applied to Lunnon's water trials show variations of the coefficient k_A of from 0.5 to 2.0, which are not excessively removed from the values quoted by previous authors. However, the data for air give values which are as high as 1,200—results which the added mass concept utterly fails to explain.

Lunnon feels that the increase of resistance due to acceleration may result from the rapid change in stream lines which could be favorable to the production of eddy motion. He points out that if this is the case, a negative acceleration should also cause an increase in C_{DA} so that Equation (2) must be modified, since it predicts a decrease

of resistance with deceleration. If C_{DA} indeed reflects the buildup or decay of vortex patterns, then the rate of change of the acceleration must be taken into consideration. The accuracy required for this type of investigation has not hitherto been attained, but it has now been made possible by a radioactive tracer method combined with a digital computer analysis [31].

In 1937, Vagner [32] attempted to extend Lunnon's data by working with a series of liquids covering a wide density spectrum. Although much care was taken to develop a suitable photographic technique, he could not measure the drag coefficient directly, but had to fall back on the added mass type of relationship as given in Equation (1). He superimposed his time-distance data on curves drawn up by assuming various k_A values, and in this way found coefficients varying from 0.5 to 1.5. Although these results show an inverse relationship between k_A and the parameter $(g\rho d^3/\mu)$, where d is the sphere diameter, g the gravitational constant, and μ the fluid viscosity, the data do not establish this in a quantitative manner.

Following the work of Vagner, the study of the acceleration effect on the drag coefficient lay more or less dormant for a period of 12 years except for the results obtained with droplets falling in air by Laws [33, 34] and correlated by Williams [35], which again suggested an increase in the drag coefficient. The post-war investigations of the acceleration effect can be divided into three very general categories, depending on whether the bodies more relative to the fluid—(a) in rectilinear but variable acceleration; (b) in rectilinear and constant acceleration; and (c) with an oscillatory motion.

Rectilinear, Variable Acceleration

Iverson and Balent [36] carefully studied the acceleration of circular discs towed by a fine weighted cable and set perpendicular to the motion, and the added mass concept completely failed to explain the large dependence of the fluid resistance on the particle acceleration. From an examination of the Navier-Stokes equations, they felt that C_{DA} should be a function of $(L_p U_p \rho/\mu)$, (U_p^2/gL_p) and $(\dot{U}_p L_p/U_p^2)$ where L_p is a characteristic length specific to the body shape. The last group $(\dot{U}_p L_p/U_p^2)$—called the acceleration modulus—was found to correlate all the C_{DA} values on one smooth curve, and no Reynolds Number dependency was apparent. They felt that their data were limited, and they planned to study the effects of deceleration, shape and finite initial velocity over a sufficient velocity range to properly establish the Reynolds Number dependency.

Keim [37] has more recently repeated and extended Iverson and Balent's work with circular discs and the data of both investigations agree very well—a situation which is perhaps unique in the reporting of acceleration drag coefficients! Keim also measured C_{DA} values for cylinders of various length-to-diameter ratios, and these showed an explicit dependency on the Re, $(\dot{U}_p d/U_p^2)$ and (L/d) parameters. In Figure 2 the authors of the present survey have replotted some of Keim's data using C_{DA} and Re as the co-ordinates, at a constant (L/d) ratio, and these clearly show the manner in which the acceleration parameter acts to displace the drag coefficient curve. One noteworthy characteristic which was also indicated by Lunnon's data is that the effect of acceleration on the drag coefficient becomes reduced as the Reynolds Number, and therefore the turbulent component of the wake structure, is increased. The effect of the (L/d) ratio on

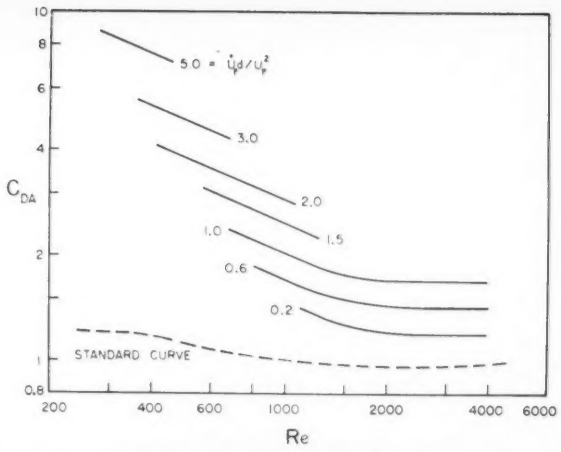

Figure 2—Drag coefficients of cylinders accelerating from rest (Keim).

the C_{DA} values was very similar to that found in steady motion. Keim's dimensional analysis derivation of the acceleration modulus is more complete than the one given by Iverson and Balent in that it predicts a dependency on the rate of change of acceleration as well as higher order derivatives of the velocity which would be correlated by dimensionless parameters of the general form $(d^{n-1}/U_p^n)(\delta^n x/\delta\theta^n)$. Keim made no attempt, however, to measure or test for the effect of the terms of higher order than the acceleration.

Working with a system similar to that studied by Keim, Bugliarello [38] published a lengthy series of results obtained with 7.6, 8.9 and 15.2-cm. spheres which were drawn by constant forces up through a stagnant pool of water. Again the added mass concept was found to be completely inapplicable, giving uncorrelated added mass coefficients which ranged from as high as 500 down to negative quantities. Bugliarello found that his results were best represented by the total drag coefficient C_{DA}. His plots of C_{DA}—versus—Re for the 7.6-cm. and 8.9-cm. spheres, though considerably scattered, are qualitatively similar to the right hand section of Lunnon's curves, and they show drag coefficients with values as high as 30, compared to the steady state value of 0.4. The results with the 15.2-cm. sphere were considerably more scattered and indicated a smaller acceleration effect; in many cases the drag coefficients had been reduced to almost half their steady state values, rather than increased as in the other two cases. Bugliarello considers that this anomalous behavior was due to the sphere boundary layer being made prematurely turbulent by surface roughness, and if correct this again indicates a reduced acceleration effect possibly brought about by an increase in wake turbulence.

The authors of this survey have replotted some of Bugliarello's data again using C_{DA} and Re as co-ordinates and the acceleration modulus as the varying parameter, and the result, shown in Figure 3, indicates the same diminishing of the acceleration effect with increasing Reynolds Numbers. The curves roughly show the same features as the cylinder results of Keim, but in Bugliarello's case the data are too scattered and limited to establish the curves quantitatively.

Bugliarello maintains, and his data seem to indicate, that C_{DA} will tend to a value of $(2/3)(\dot{U}_p d/U_p^2)$ at very high values of $(\dot{U}_p d/U_p^2)$, a result which can be derived from

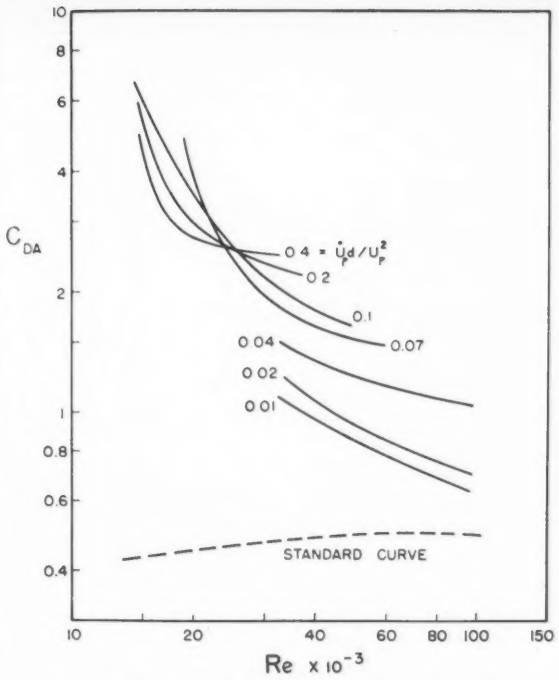

Figure 3—Drag coefficients for accelerating spheres (Bugliarello).

potential flow considerations, but as will be shown, the flow about a sphere is described by potential theory only at the very beginning of an acceleration, and the reported tendency may have been due to the fact that the high acceleration data always corresponded to the beginning of the sphere motion.

The rectilinear but varying acceleration encountered by particles falling or being drawn through a stagnant fluid represents but one of the many possibilities which may occur in solids-gas systems. For example, a particle at rest inserted into a rapidly moving gas stream would experience an *absolute* acceleration until an equilibrium velocity is attained, but considering its behavior relative to the fluid, it instantaneously has a finite Reynolds Number which diminishes as the particle decelerates relative to the fluid to the equilibrium velocity. On the other hand, a particle fired into a stagnant fluid from a nozzle with a velocity greater than its terminal velocity would experience both a relative and absolute deceleration, and extrapolation of drag results obtained from the former system to the latter would not be valid, particularly since the acceleration drag mechanism is probably influenced by both relative and absolute effects as well as by their signs and magnitudes.

The system consisting of a particle injected from rest into a moving gas stream most often occurs in the feeding zone of solids-gas apparatus and its investigation is reported by Ingebo [39, 40] in a recent series of papers dealing with the acceleration of small droplets and solid spheres injected as a cloud with a negligible entrance velocity into an air stream moving with velocities of 140 to 180 feet per second. Under these conditions, the particles had accelerations as large as 60,000 ft./sec.^{2}—a value far greater than the maximum of 32 ft./sec.^{2} for particles falling into a stagnant fluid. The velocities were measured at fixed stations from 5 to 32 cm. downstream from the injection point by a specially-designed droplet camera.

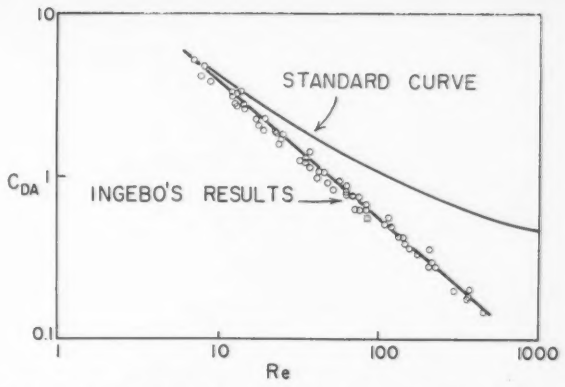

Figure 4—Drag coefficients of spheres entrained in a moving air stream (Ingebo).

Surprisingly all the data, regardless of the acceleration magnitude or whether they were obtained with solid spheres or liquid droplets, fell on the single line shown in Figure 4, and were correlated by the relationship

$$C_{DA} = 27/Re^{0.84} \quad \ldots\ldots\ldots\ldots\ldots\ldots\ldots\ldots (5)$$

for the entire experimental range of Reynolds Number from 6 to 500. At Re = 500, C_{DA} had dropped to 0.15, compared to the steady state value of 0.55, and if this trend can be shown to extend to higher Reynolds Numbers, the drag coefficients will fall to very small values. The particle drag was not affected by the presence of other particles, since a ten-fold increase in their concentration did not bring about any noteworthy alteration to their velocities.

Ingebo's results are unique in several respects: firstly, they show a decrease in the drag coefficient, rather than the increase due to acceleration reported by most workers for this Reynolds Number region; secondly, they show an increased departure from the standard curve as the Reynolds Number increased, whereas all the other acceleration data discussed so far show a decreased acceleration effect as the Reynolds Number is increased; and finally all the drag data regardless of the magnitude of the associated accelerations fall on a single curve rather than on the individual curves usually obtained for different accelerations, although, this may have resulted from the experimental system being one in which the Reynolds Number and the acceleration could not be varied independently and the highest accelerations are here associated with the highest Reynolds values obtained. The data are also complicated by the presence of an unspecified amount of free stream turbulence and by some uncertainty as to the accuracy of the fluid velocity determinations; nevertheless, they dramatically underline the necessity of investigating all the possible non-steady particle velocity systems on an individual basis.

Fledderman and Hanson [41, 42] carried out similar investigations, in which a photographic technique was used to observe spray droplets entrained and accelerating in air streams moving from 50 to 70 ft./sec. The droplets had relative Reynolds Numbers varying from 20 to 100 so that their behavior, according to Ingebo's findings, should not differ from that of the solid spheres. The data shown in Figure 5 indicate a clear dependence on air velocity, unlike those given by Ingebo. The results are surprisingly low, at times representing a decrease of one thousand percent from the standard curve values. Fledderman and Hanson felt that this was due to evaporation

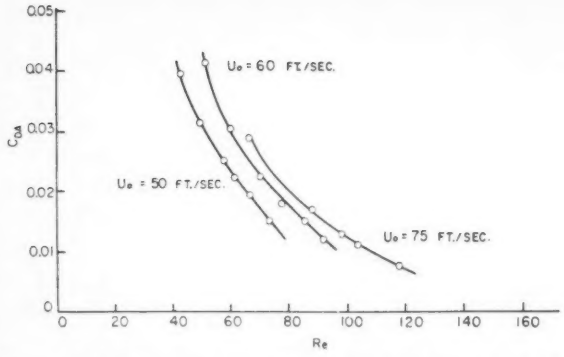

Figure 5—Drag coefficients for spray particles entrained in a moving air stream (Fledderman and Hanson).

occurring at the droplet surface, but this possibility seems to have been ruled out by Ingebo's work, which involved both evaporating and non-evaporating droplets. The particle velocity data may have been in error since they were not obtained directly, but were derived from Froessling's mass transfer equation [43] relating the droplet velocity to the photographically determined decrease of diameter with time. The application of this equation to sprays of droplets has been more or less verified by a recent work by Manning [7], so that the error in the drag data is probably not excessive.

The large difference between the data of Ingebo and those of Fledderman and Hanson remains to be explained, as well as the complete contradiction between these results which indicate a drastic reduction in the drag as compared with the increase caused by acceleration in the other experiments. The fluid turbulence intensity in Fledderman and Hanson's test section was found to be of the order of two percent (based on measurements taken when no particles were present), whereas the turbulence in Ingebo's apparatus, while not measured, was probably much lower because of the presence of a 50 x 40-mesh screen in the upstream section. It may be that the disagreement in part reflects a reaction to varying *relative* intensities and scales of turbulence, but the information from the experiments is not sufficient to establish any dependency. A second complication may result from the necessity to correlate all acceleration drag data as a function of a time parameter which is related to the total time allowed for the build-up of the boundary layer and wake of the particle.

Rectilinear, Constant Acceleration

As discussed in the previous section, the drag measurements taken using constant driving forces such as the pull of gravity or of a weighted string attached to the body, as well as those measured on particles moving freely through a gas stream, are always associated and thereby complicated by changing accelerations. Luneau [44, 45, 46, 47] in 1948 initiated a program which removed this complication by using a towing device which could be set to pull the test body at different constant accelerations, and the required drag force was instantaneously and continuously recorded throughout each run by means of strain gauges. Experiments with circular discs set perpendicular to the motion showed two categories of drag behavior. In the first the increase of drag remained roughly proportional to the acceleration magnitude, but in the second, the drag was initially much larger but eventually dropped to the values found in the first case. Insufficient data were reported to indicate any explicit

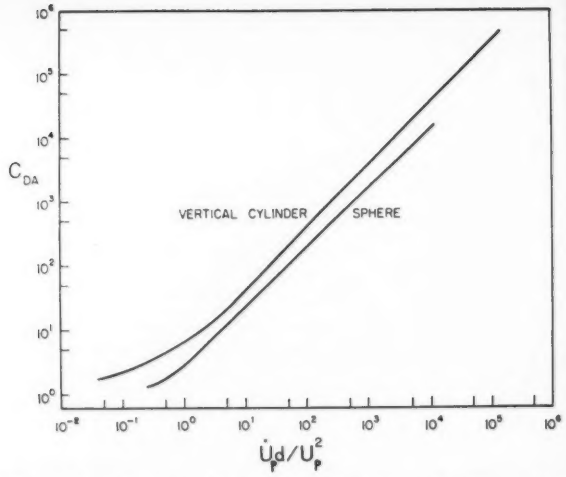

Figure 6—Drag coefficients of cylinders and spheres suspended in an oscillating fluid (Crooke).

Reynolds Number or time dependency. For circular cylinders, however, C_{DA} was actually less than C_D for $Re < 10^3$, but surpassed it in the region $10^3 < Re < 10^5$—the increase due to the acceleration increasing as the cylinder diameter *decreased*, and in the region about 10^5 Luneau was unable to obtain reproducible results. Laird and Johnson [48] in 1956 also reported a long-range program to study the acceleration effects on the drag coefficient, and their preliminary results with cylinders of finite length towed at constant acceleration through water did not show any Reynolds Number correlation, and only showed a slight correlation with the acceleration parameter. The data are very scattered, but they generally show that for the Reynolds Number range of 1.5×10^4 to 1.25×10^5, C_{DA} went from 0.6 to 1.7 as $(\dot{U}d_p/U_p^2)$ went from −0.04 to 0.18 as compared with the steady state value of 0.85. These data are among the first to result from studies of the effects of deceleration, and the reduction of the drag coefficient in this case is particularly noteworthy. Data from constant acceleration experiments are just beginning to accumulate so that even qualitative conclusions cannot as yet be made, other than that the results obtained with varying acceleration differ from those in which the acceleration is held constant.

Acceleration in Oscillatory Motion

The post-war period has given rise to the renewed investigation of the acceleration effects on particles oscillating in a fluid. These experiments are divided into two groups: in the first, the body is held fixed while the ambient fluid is given a specific oscillation—in some cases resembling the motion of waves on a fixed pier; in the second, the test body moves to and fro usually by attachment to a system of springs. The important consideration is that in both systems the continual reversal of the relative flow direction does not allow the flow patterns around the particle to develop as they would in rectilinear motion, and the particle continually enters a flow regime which has been disturbed by the previous cycle; nevertheless, the data obtained shed further light on acceleration phenomena in general, and will be particularly useful in the consideration of the behavior of small particles imbedded in large scale turbulent flows. They are also important in explaining results being obtained with solids-gas systems subjected to sonic energy.

(i) *Fixed Bodies in Oscillating Flows*

The forces on bodies immersed and held fixed in an oscillating fluid have been conventionally correlated by a modified version of Equation (1), which has the form:

$$R_A = C_M V_p \rho \dot{U}_p + 1/2\, C'_D \rho A_p U_p |U_p| \quad \ldots\ldots\ldots (6)$$

where $|U_p|$ is the positive numerical value of U_p and the coefficient C_M is generally taken as being equal to $(1 + k_A)$, the addition of 1 to the added mass coefficient resulting from the fact that in this system the entire fluid –rather than the body–is accelerating, and C_D' is a coefficient which is not to be confused with either the steady state C_D or the total acceleration drag coefficient C_{DA}. This equation gives the erroneous impression of being theoretically well founded, but it is actually based on an intuitive extrapolation from inviscid fluid behavior which assumes that the drag forces during unsteady motion at finite Reynolds Numbers can be parceled off into two discrete packages which are independently related to the acceleration and velocity, respectively. It also gives rise to the possibly unsound practice of solving for two experimental force coefficients from only one experimental force determination, thereby complicating the interpretation of the data.

Very often the values of C_M and C_D' are obtained by considering the oscillation to be sinusoidal, so that the $1/2 C_D' A_p \rho U_p |U_p|$ term is zero when the U_p value drops to zero at the phase angles 90° and 270°, and similarly the C_M term is eliminated at 0° and 180° when the value $\dot{U}_p$ becomes zero–needless to say, the values of C_D' and C_M obtained at 0 and 90° respectively do not generally correspond with those indicated at 270° and 360° as they would if the concept was valid. In other instances, the value of C_M employed in the calculation of C_D' is the average obtained during the whole series of trials, and a third practice uses the added mass coefficient predicted by inviscid flow theory.

In a series of papers, Morison and O'Brien [49, 50, 51], in conjunction with others, reported results with fixed cylinders and spheres, and Equation (6) when applied to the results for cylinders showed variations of C_M from 1.4 to 1.6. C_D' was found to fall with increasing Reynolds Numbers from about 40 at $R_e = 1{,}000$ to close to the steady state value at $Re = 10{,}000$, and there was considerable scatter in the data, C_D' varying by as much as 700 percent at a constant Reynolds Number. Crooke [52] reanalyzed Morison's data, plotting the total drag coefficient C_{DA} as a function of the acceleration modulus $(\dot{U}_p d/U_p^2)$. The results for spheres and cylinders immersed in oscillating fluids are shown in Figure 6, and the correlation is surprisingly good, showing a considerable improvement over that given by Morison. Crooke found no clear Reynolds Number trends for the range covered but at the lower values of the acceleration modulus rough qualitative tendencies which are similar to those found with rectilinear motion are indicated. At about the same time, McNown [53] presented a paper dealing with preliminary investigations of the forces on flat plates and lenticular cylinders fixed in a fluctuating flow, and he proposed a correlating equation which is an improved form of Equation (6) in that the added mass coefficient is acknowledged as being a function of time, giving the relationship:

$$R_A = \rho V_p \dot{U}_p + V_p \rho \delta (k_A U_p)/\delta\theta + (1/2) C_D' \rho A_p U_p^2 \quad \ldots\ldots (7)$$

McNown reasoned that since C_D' and k_A both depend on the particle shape there must be a unique relationship between them, and a single curve with k_A and C_D' as coordinates was theoretically calculated from an extension of the Kirchhoff approach discussed in Part II of this series, and it was incorporated with an artificial model of the flow in which it was necessary to ignore the complexities of the wake mechanics. Assuming the curve to be valid, he then tried out different variations of k_A with time until one was found which predicted the variations of force observed. The degree with which the k_A vs C_D' relationship corresponds to reality is difficult to establish, particularly since the remainder of the analysis into which it is inserted may not be valid for real fluids.

Wiegel, Beibe and Moon [54] measured the forces on cylinders submerged in actual ocean waves whose velocities were experimentally recorded. In spite of Crooke's success with the overall drag coefficient the authors here again analyzed their results by the use of Equation (6) and obtained a very large number of points, which were unfortunately accompanied by a very wide scatter of coefficients showing a decrease as well as an increase of C_D' with acceleration. The authors felt that the results differ from those obtained in laboratory trials because of the variable turbulence present in the ocean waves. In conclusion, they re-analyzed a small portion of their data using the total drag coefficient and here obtained moderate success and the results fell between the curves given by Crooke and Keim, but they unfortunately did not have time to re-analyze the bulk of their data in this way.

Borgman [55] has developed equations in vectorial and matrix notation which would allow the drag force data already obtained to be applied to cylinders which were oriented in any arbitrary manner with respect to the oscillation direction, but the results must be checked by experiment, since the method implies no alteration of the fluid dynamic behavior due to the orientation.

Very recently, Keulegan and Carpenter [56], in what is perhaps the finest work of its kind, measured the forces on cylinders and plates fixed in an oscillating fluid. They modified Equation (5) to the form:

$$R_A = C_M V_p \rho \dot{U}_p + 1/2\, C_D' A_p \rho |U_p| U_p + \Delta R \quad \ldots\ldots (8)$$

where R_A is the instantaneous drag force and the coefficients are here the averaged values taken over the entire cycle of oscillation. ΔR is a supplementary force which makes up for the fact that C_M and C_D' are averaged rather than instantaneous values. A very important contribution made by this paper is the introduction of the fundamentally meaningful reduced time parameter $(U_m T/d)$, U_m being the maximum fluid velocity of the cycle and T its period, and this parameter is proportional to the number of diameters travelled by the fluid in one direction before the flow reverses, so that it reflects on how much time is given to the boundary layer and wake to develop. This information may relate the oscillating flow problem to the frequency of the turbulent fluctuations in the case of small particles imbedded in very large scale turbulent fields.

The applicability of the time parameter is illustrated by the remarkable degree to which it correlated the resistance coefficients. Smooth curves of C_D' and C_M vs. $(U_m T/d)$ were obtained for both cylinders and plates with the results for the various trials all falling close to

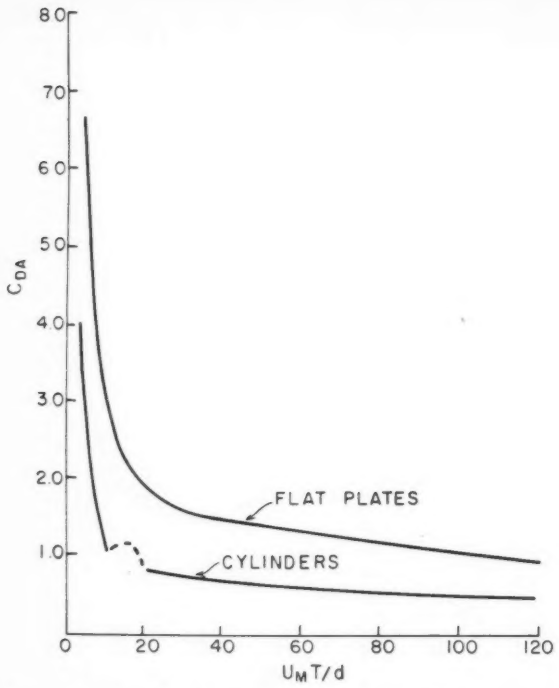

Figure 7—Drag coefficients of flat plates and cylinders fixed in an oscillating fluid (Keulegan).

a single curve for each shape. Reasonable explanations were given for the different C_D' curves obtained for cylinders and for plates, but this could not, however, be done for the added mass coefficients, which should have remained constant. Although the authors placed their main emphasis on the Equation (8) type of analysis, plots were also given of C_{DA} as a function of the time parameter, and the correlation was excellent. As is shown in Figure 7, the data for cylinders and plates both follow similar curves in which the coefficients decrease rapidly at first and then more gradually to the steady state value as the time parameter is increased. Surprisingly absent is a Reynolds Number effect, but a wider experimental range including different bluff body shapes will now be required to confirm the uniqueness of the $(U_m T/d)$ group as a correlating parameter for oscillating motion. A discussion of this parameter is continued in the following section on the fundamental aspects of the acceleration problem.

(ii) *Oscillating Bodies in Stagnant Fluids*

The post-war investigations of the force system on a body oscillating in a fluid at rest have not been as actively pursued as the category just discussed. Carstens [57], using a table-tennis ball submerged in various viscous fluids and attached to an oscillating system of weights, felt that he could best describe the forces on the sphere by an expression which is equivalent to Equation (1), except that the (U_p^2) term was replaced by a viscous damping force which was assumed to be proportional to U_p rather than U_p^2, resulting in the expression:

$$R_A = k_A \rho V_p \dot{U}_p + k_s U_p \qquad (9)$$

where k_s is a "viscous damping" coefficient. Following a dimensional analysis, Carstens is led to believe that both k_A and the ratio of $(k_s U_p)$ to the viscous drag predicted by Stokes Law (the ratio being given the symbol N_2) will be functions of the parameters $N_1 = \sqrt{(8\mu/\rho\omega)}/d$, where ω is the angular velocity of the oscillation which is assumed to be sinusoidal and $2E/d$ where E is the maximum amplitude of the oscillation. N_2 was found to decrease and the added mass coefficient k_A was found to increase with increasing values of N_2, but more experimental data covering a broader experimental range are required before any generalizations can be made.

Stelson [58, 59] felt that the scattered added mass values reported in the literature were more the result of inappropriate measurement rather than a breakdown of the added mass concept. Stelson's experimental technique consisted of attaching the submerged test bodies to a rigid bar which was then vibrated at the natural fundamental frequency of the combined system. The system was first vibrated in air using varying masses for the test bodies so that a relationship between the body mass and the frequency of the vibration was found. The added mass of a given body was obtained by vibrating it when submerged in water and then noting the mass corresponding to the new vibration frequency. Stelson ascribed the apparent increase in mass as being entirely due to the added mass of the body. The amplitudes of the oscillations in these experiments are very much smaller than are usually obtained in experiments with oscillating bodies, so that the fluid system about the body does not have time to depart from the potential flow pattern, and for this case alone the classical hydrodynamic treatment may provide a good approximation.

Stelson obtained results for a variety of shapes as well as spheres, and for the latter, k_A was found to be equal to 0.51, which almost coincides with the theoretical prediction. For cubes, k_A was found to be equal to 0.67 for both the broadside-on and edge-on motion, and although there was no theoretical solution available for the cube, Stelson points out that Polya [60] and Szego [61] had shown that the theory predicts that the added masses in both positions should agree with each other. The k_A values for rectangular plates with varying length-to-width ratios and for circular cylinders with different length-to-diameter ratios fell on smooth curves extrapolating to values predicted by potential flow theory. The results obtained, together with the analysis employed, seem to be valid for the one extreme of the oscillation problem in which the amplitude is negligible. The experiments previously cited point out, however, that with increasing amplitude the problem rapidly enters into a regime in which the empirical and analytical difficulties reflect the complexity of the attendant flow characteristics.

Fundamental Investigations of Accelerating Phenomena

The following discussion is divided into two sections: the first deals with attempts to elicit information concerning the changing flow fields and drag coefficients in unsteady motion by approximate solution of the pertinent Navier Stokes Equations, and the second discusses the empirical investigation of the effect of non-steady motion on the boundary layer and wake properties.

Theoretical Investigations

(i) *Reynolds Numbers < 1*

If the system is confined to one in which the accelerations are very moderate, and the particle Reynolds Number is always less than one, it becomes possible to overcome the difficulties introduced by the non-linear

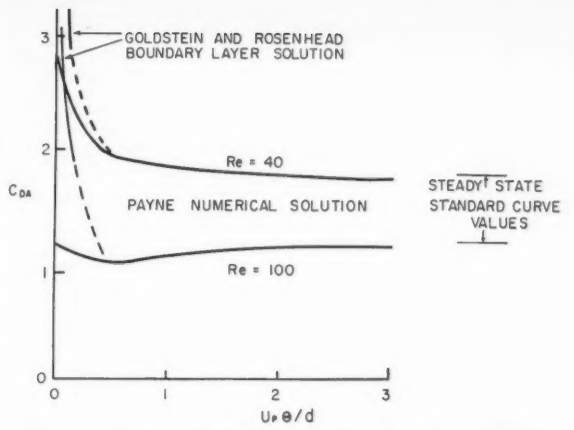

Figure 8—Drag coefficients for a cylinder impulsively accelerated from rest (Payne).

terms of the Navier Stokes equation, and calculations by Basset [62], Boussinesq [63] and Oseen [64] show that the resultant drag force on a particle starting from rest and accelerating in a stagnant fluid is given by:

$$R_A = (1/2)V_p\rho\dot{U}_p + 3\pi\mu d\, U_p + 3\pi\mu d^2 (\pi\rho/\mu)^{1/2} \int_{\theta_o}^{\theta} \left[\dot{U}_p(\theta_1)/(\theta - \theta_1)^{1/2}\right] \delta\theta_1 \ldots (10)$$

The first right hand term is identical to the added mass resistance predicted by classical hydrodynamics and the second term coincides with the steady-state drag given by Stokes Law. The third term shows that even in the idealized Stokes Law region the drag force will depend on the previous history of the particle motion. Tchen [65] has generalized Equation (10) for systems where both the particle and fluid are undergoing acceleration, but the forces will become complex functions of the Reynolds Number as well as the acceleration parameter ($\dot{U}_p d/U_p^2$).

More recently, Pearcey and Hill [66] have dealt with the case of a spherical particle which is instantaneously accelerated from rest at $\theta < 0$ to a uniform velocity U_p at $\theta > 0$. Their solution employs the Oseen approximation to the inertia terms (see Part I) so that it is limited to Reynolds Numbers of less than unity. For small values of the time parameter $T_\theta = (4\mu\theta/\rho d^2)$, the drag force is given by:

$$R_A = 3\pi\mu d\, U_p \times \left[1 + (\pi T_\theta)^{-1/2}\left\{1 + (3Re^2T_\theta)/40 + 0(Re^4T_\theta^2)\right\}\right] \ldots (11)$$

and for large T_θ:

$$R_A = 3\pi\mu d\, U_p \times \left[1 + (\pi T_\theta)^{-1/2}\left\{25/2Re^2T_\theta + 0(Re^{-4}T_\theta^2)\right\}\right] \ldots (12)$$

The solutions indicate that the drag force in impulsive acceleration is made up of three components: the first is identical with the steady state Stokes Law drag, the second is infinite at the start of the motion and decreases as $\theta^{1/2}$, and the third component acts only at the instant that the impulsive motion is initiated. Equations (11) and (12) suggest that in the region of extremely low Reynolds Numbers the effect of the non-steady motion on the drag coefficient will decrease with decreasing fluid densities, and specific solutions for the trajectories of small spheres in air should show only a small effect due to the acceleration compared to the large effects noted experimentally in air at higher Reynolds Numbers.

(ii) *Reynolds Numbers > 1*

There does not seem to be any overall unsteady-state drag solution for the post-wake-forming Reynolds Numbers for the sphere system, so that, as before, recourse is made to work done for the simpler case of the cylinder. Payne [67] using a finite difference numerical approach similar to the methods employed by Kawaguti [68] and Thom [69] for the steady state cylinder case (see Part II), obtained specific solutions for impulsive motion occurring at Reynolds Numbers of 40 and 100. The solutions are plotted in Figure 8 showing the drag coefficient to be a unique function of the Reynolds Number and the time parameter ($U_p\theta/d$), the latter being equal to the number of diameters traversed by the cylinder since the initiation of the motion. The drag drops rapidly at first and then gradually to the steady state value in a surprisingly short period of time, requiring only a distance of about three diameters to come to within 2% of the value given by the standard curve. At the beginning of the motion the ambient boundary layer is very thin and the intervals employed in the numerical computation are too large to obtain accurate values of C_{DA}. For this region Payne reverts to a boundary layer solution offered by Goldstein and Rosenhead [70] which predicts that for θ tending to zero:

$$C_{DA} \simeq 4(\pi d/ReU_p\theta)^{1/2} \ldots (13)$$

the skin friction accounting for half of the total. This boundary layer solution and the others, which will soon be discussed, are not reliable after separation occurs (for the cylinder this happens when approximately 0.2 diameter has been traversed) so that Payne has joined the valid regions of both solutions with a dashed line. It is noteworthy that the solutions show no dependency on the fluid density, beyond that contained in the Reynolds Number—in contrast with the equations previously cited for Reynolds Numbers of less than unity—and the total drag coefficient was easily represented by a single smooth curve. Payne expects to extend his treatment to higher Reynolds Numbers by the use of improved electronic computers and the predicted flow fields can then be compared with empirical measurements already available for Reynolds Numbers in the vicinity of 600.

An attempt has been made by Schwabe [71] to obtain an analytical solution for the pressure fields about impulsively-accelerated cylinders at higher Reynolds Numbers, using potential flow theory. The results were compared with experiment, and as in the case with steady motion this approach was moderately successful for the frontal region up to the wake, but the wake region had to be replaced by an artificial model to allow the calculation of the non-wake region. As the time increased, the discrepancy between the calculated and observed flow patterns became larger and the region of applicability of a potential flow analysis was shown to be restricted to the beginning of the motion.

(iii) *Boundary Layer Solutions*

The boundary layer solutions available for impulsive motion are valuable in two respects, in that they describe the fluid motion at the very beginning of the event, and they predict the time interval between the initiation of motion and the separation of the boundary layer.

Blasius [72] launched the mathematical attack on the problem of the boundary layer build-up on a cylinder impulsively accelerated from rest and his approximate solution indicated that separation will occur after the cylinder had moved the short distance of 0.15 diameter. He describes the initial few moments as being a transformation from a potential state of flow with a boundary layer of zero thickness developing initially through frictional processes and subsequently through the convective terms in the equations of motion. The boundary layer soon thickens and separates, and it is important to realize that the boundary layer solutions are no longer valid past this point. For the case of constant acceleration from rest, Blasius found that separation occurred when only 0.6 diameter had been traversed so that generally the period of application of boundary layer solutions is a particularly short one. The wake build-up is shown to occur almost at the start of the movement in an interval which would not be detected in macroscopic studies. Improvements to the Blasius solutions have been made by Goldstein and Rosenhead [70] but the corrections to the time intervals for separation are minor.

Boltze [73] provided an approximate solution to the boundary layer equations for an impulsively-accelerated sphere, and the results were similar to those obtained with cylinders with separation occurring after 0.2 diameter had been traversed. More recent works [74, 75, 76, 77, 78, 79, 80] have provided refined solutions which include treatments with arbitrary time-dependent velocities with particular emphasis being placed on the flow near the front stagnation point, and they emphasize the rapidity of the boundary layer build-up to the point where separation first occurs.

(iv) *Solutions for Oscillating Systems*

The analytical treatment of a body oscillating in a fluid is simplified if the motion is restricted to instantaneous Reynolds Numbers which are much smaller than one, and for this case Lamb [81] has derived a formula giving the value of the added mass coefficient as:

$$k_A = 0.5 + (18/4d)(\mu/\pi f\rho)^{1/2} \quad \ldots\ldots\ldots\ldots (14)$$

where f is the frequency of oscillation. For finite Reynolds Numbers the flow system becomes far more complex and the treatment has been thus far usually restricted to oscillations with amplitudes which are smaller than the characteristic diameter of the immersed body and to systems in which vortex shedding does not occur. The boundary layer solutions for bodies fixed in an oscillating fluid are closely associated with the experimental observations of the authors concerned so that these will be taken up in the experimental section. Solutions for the boundary layers of cylinders oscillating in an on-coming fluid have been limited to the frontal region of the bodies and have been given by Glauert [82] for oscillations transverse to the stream and by Lighthill [83] for oscillations parallel to the stream.

Experimental Investigations

One of the most valuable insights into the processes occurring during impulsive acceleration has resulted from an investigation by Schwabe [71]. Using minute particles to trace and record the velocity and direction of movement of the components of the flow, he succeeded in obtaining a series of photographs showing the progressive evolution of the ambient flow structure from the very beginning of the motion. These tracer velocity measurements were sufficiently accurate to allow the calculation of the entire

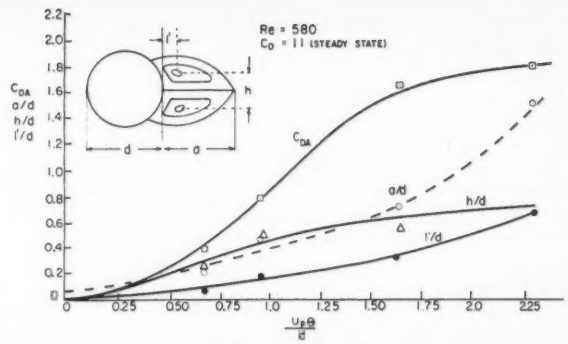

Figure 9—Drag coefficients and wake dimensions for a cylinder impulsively accelerated from rest (Schwabe).

pressure distribution occurring at a given instant, which is not possible with a pressure probe because of the finite time required for even a single measurement. Integration of the pressure field yielded the acceleration drag coefficients and these, together with the dimensions of the various wake components for a constant Reynolds Number of 580, are shown in Figure 9, as a function of the time parameter $\theta_S = (U_p\theta/d)$, which represents the number of cylinder diameters traversed from the start of the motion. It would seem that the drag coefficient rises rapidly from zero at first and then more gradually to a maximum which is almost twice the steady state value. It may be inferred that the eventual decrease of C_{DA} to the steady state C_D is probably a very gradual one, although this was not ascertained by Schwabe, since the experimental system did not allow measurements beyond $(U_p\theta/d) = 3$. There are several noteworthy discrepancies between this result and the analytical solutions cited previously. Although the latter predict an infinite drag at $\theta = 0$, descending rapidly as the flow develops, Schwabe's results indicate the reverse. This may be partly due to Schwabe's result giving only the form drag, omitting the skin friction component. The form drag, according to the boundary layer solution, should also be infinite at $\theta = 0$ but paralleling the case of Payne's calculations, the computational intervals used in the evaluations of the pressure are too large to detect the gradients occurring at the start of the process when the boundary layer is extremely thin. More important—but more difficult to explain—is the fact that Payne's calculations suggest the period of increased drag coefficient occurs in an interval which is not greater than $0 < (U_p\theta/d) < 0.5$, for Re = 40 and 100, the interval as well as the drag increase due to acceleration tending to decrease with increasing Reynolds Numbers. Schwabe's experimental force determinations – which can only be conservative due to the omission of the skin friction component–show a much longer period of abnormal drag behavior as well as a larger increase in the drag coefficient, this being more compatible with the results obtained in the macroscopic investigations. A more direct comparison will be available when Payne obtains results at higher Reynolds Numbers.

Recalling that Ingebo's drag determinations were carried out under conditions which initially approximate impulsive acceleration, there should be some agreement with the fundamental investigations of Payne and Schwabe. Particularly difficult to explain is the decrease in drag shown in Figure 4. Although Schwabe does record decreased drag at the initiation of the motion (this trend being subject to revision when the boundary layer contribution is taken into account more fully) the effect is

limited to the time taken for the particle to travel one diameter (at the most), after which increased drag forces are shown.

The picture is further complicated by a reanalysis of Ingebo's work given by Mercier [84], according to which the coefficients k_4 and k_5 in Ingebo's correlating equation:

$$C_{DA} = k_4/Re^{k_5} \quad \ldots\ldots (15)$$

are not equal to 27 and 0.84 respectively, as had been reported by Ingebo, but vary widely, k_4 having values which range from 0.5 to 2. Since in Ingebo's apparatus there were four observation stations placed downstream from the injection point (designated as 0,1,2,3), Mercier integrated the equation of motion which incorporated Equation (15) and he solved for k_4 and k_5 by using either the consecutive intervals 0-1, 1-2, or 1-2, 2-3. This procedure is somewhat inconsistent since on the one hand it assumes that the coefficients remain constant over the interval of integration, whereas it was shown that in a given experiment k_5 would sometimes have the value of 0.5 when obtained from the interval 0-2, and the value of 2 for the interval 1-3, which leads to the suggestion that k_5 may vary continuously throughout the interval 0-3, possibly having values less than 0.5 and greater than 2. Nevertheless, Mercier suggests that the accelerating particles are initially in a dynamic regime in which $k_5 = 0.5$ and they then enter into a region in which $k_5 = 2.0$. The transition between the two regimes supposedly occurs abruptly at points whose loci describe the curve:

$$C_{DA} = 16/Re^{0.75} \quad \ldots\ldots (16)$$

Furthermore, Mercier finds that the drag coefficients at the beginning of the motion fall on the curve:

$$C_{DA} = 75/Re \quad \ldots\ldots (17)$$

and he explains this as being a result of the flow structure around the particle when it is being impulsively accelerated. This assertion is contradicted by the available fundamental studies since Equation (17) predicts a rapidly increasing lowering of drag coefficients as the Reynolds Number increases above 40. Although Mercier's analysis seems to fit Ingebo's results it may be that the results are subject to systematic errors (as was suggested by Ingebo himself) and to complicating phenomena other than acceleration, so that it may be too early to attempt to present quantitative fundamentally-meaningful relationships without the further accumulation of experimental data.

A series of fundamental studies of the wake system of a flat plate accelerating at a constant rate from rest was started by Batailler in 1956 [85, 86] with the aid of an elaborate photographic technique which allowed fine-scale observations to be taken of the velocity and acceleration of the wake velocity field as a function of time. This was accomplished by inserting minute tracer particles into the flow and then illuminating them with a closely spaced series of xenon lamp flashes of known time duration. At the start of the motion, the flow in this investigation was also found to be potential but as the velocity increased there was a growth of stagnant fluid at the edges of the plate and eventually periodic discharges of eddies developed. In a second study, stronger accelerations were employed, and here there appeared a strange chain of discharge from the plate edges of small stagnant pools of fluid which eventually fed into the large standing eddy at the plate rear. The drag coefficient was found to be more than twice the steady state value.

Using dimensional analysis, Batailler next attempted to find a parameter which could be used to characterize the wake dimensions in an unsteady system, and this led to the development of the dimensionless time group:

$$\theta_B = \theta(\dot{U}_p/d)^{1/2} \quad \ldots\ldots (18)$$

The changing wake length L_W (here taken as the distance from the rear face of the plate to the rear separated stagnation point) was very well correlated for the range of accelerations and plate diameters employed by the relationship:

$$L_W/d = 0.5\,\theta_B \quad \ldots\ldots (19)$$

with surprisingly little deviation of the data from this straight line relationship. These investigations are as yet preliminary but the θ_B time-parameter should prove to be very useful in correlating the accumulating data on wake dimensions and drag forces with constant acceleration rates. It is interesting to note that θ_B is in some ways the finite acceleration analogue to Schwabe's impulsive acceleration time-parameter, $\theta_s = (U_p\theta/d)$ which is equal to the distance, in body diameters, traversed since the start of the motion. In the simplified case of constant acceleration, the relationship S = distance traversed = $1/2\ \dot{U}_p\theta^2$ can be substituted into the time group given by Equation (18), the latter is then found to be proportional to the square root of the distance, in body diameters, traversed since the start of the motion. Similar substitution shows that if the acceleration is constant, the acceleration parameter $(d\dot{U}_p/U_p^2)$ is inversely proportional to the number of body diameters traversed, so that in the constant acceleration case alone correlation by θ_B and $(d\dot{U}_p/U_p^2)$ becomes synonymous, although different curves will be obtained.

An exacting study of the vortex system formed during the oscillation of a body in a fluid has been made by Andrade [87, 88] during the course of an investigation into the use of solid particles as a means of measuring the modes of the sonic vibration of gases by the familiar Kundt's tube method. Both cylinders and spheres with diameters as low as 81 microns were individually placed into a column of gas which was vibrated at various frequencies and amplitudes. The flow systems surrounding the suspended spheres were made visible by the plane illumination of minute smoke particles, and when the Reynolds Number of the oscillating gas flow entrained (calculated by using the maximum relative velocity U_m) exceeded a critical value there was clearly revealed not one but two vortex rings at opposite ends of the plane of vibration. Oddly enough, the flow in the vortices did not oscillate but was steady, and furthermore it circulated in a direction opposite to that which occurs in the steady state case. Andrade found that for the larger spheres employed (0.2 cm. $< d <$ 0.6 cm.), the Reynolds Number for wake formation, Re_w, was a function of the ratio of the oscillation amplitude E to the particle diameter d, regardless of the frequencies (see Figure 10). For the small spheres (0.025 cm. $< d <$ 0.042 cm.) there was no dependency on the (E/d) ratio at all, even though it was varied over a large range, and Re_w had a constant value of 6 which is surprisingly close to the value obtained for steady flow.

Assuming that the results are not affected by support interference, the different behavior noted with small particles as compared with large ones raises a very important

point regarding the application of data obtained from experiments with the latter to the small particles occurring in solids-gas systems. Andrade offers a possible explanation for the difference by referring to a mathematical solution for the boundary layer thickness in oscillatory motion given by Lord Rayleigh [83], noting that the ratio of the boundary layer thickness calculated from this solution to the particle diameter is much larger for the small spheres than it is for the large ones. This suggests that unsteady flow phenomena observed with large bodies must be confirmed by small particle experimentation before generalizations can be made.

Schlichting [90] in an investigation with cylinders which was similar to Andrade's, obtained photographs which showed the same vortex formation, and he succeeded in providing a boundary layer solution by a method of successive approximations which was in fair agreement with Andrade's results, but it also predicted an inner vortex system in the immediate vicinity of the cylinder which moved in the opposite direction to the outer one. Its presence had not been observed by either Andrade or by Schlichting himself. At about the same time, Carriere [91, 92] studying a similar system found that the vortex which he observed corresponded to the ones found by Andrade and Schlichting, but the direction of movement was reversed.

More recently there has been a flurry of activity by workers in acoustics seeking a more accurate description of this oscillation phenomena—referred to by them as "acoustic streaming". Skogem [93] and West [94] continued Andrade's experiments with cylinders and detected the presence of the inner vortex predicted by Schlichting. Westervelt [95] concluded that the direction of flow of the outer vortex depended on the amplitude-to-body diameter ratio (E/d), while Andres [96, 97] experimenting with cylinders found that at low values of the Reynolds Numbers (based on maximum relative velocity) only the inner vortex system appeared, but the outer flow developed when the (E/d) ratio or Re was increased. Andres proceeded to solve the boundary layer equations for large and then small Reynolds Numbers (using the Oseen approximations for the latter) and the observed flow patterns were indicated by the solutions for low values of the velocity amplitude. The analysis suggested that the type of flow occurring was characterized by the group $(\mathrm{Re}\ E/d)^{1/2}$. The solution using the Oseen approximation may not be valid since Westerveld [38] has developed a proof showing that the use of Oseen's approximation to derive the flow field in the vicinity as an oscillating object is, in the words of the author, "useless".

Experimental work with cylinders has been continued by Holtsmark et al [99], Rane et al [100] and Skavlem and Tjotta [101], and with spheres by Lane [102]. Skavlem and Tjotta improved the solution of the Navier Stokes equations and obtained very good agreement with Holtsmark's observations. Lane has modified the method of solution to deal with spheres and he showed that there was a good similarity between the properties of the two flows. In his experiments with spheres he was careful to check for possible suspension interference and was able to avoid this by limiting his diameter range to a minimum of 3/16-in. Although there was fair agreement between experiment and his theoretically predicted boundary layer thickness, closer agreement of streamlines—especially at the lower oscillation frequencies has since been obtained by Thrasher and Westervelt [103] who have altered the theoretical treatment.

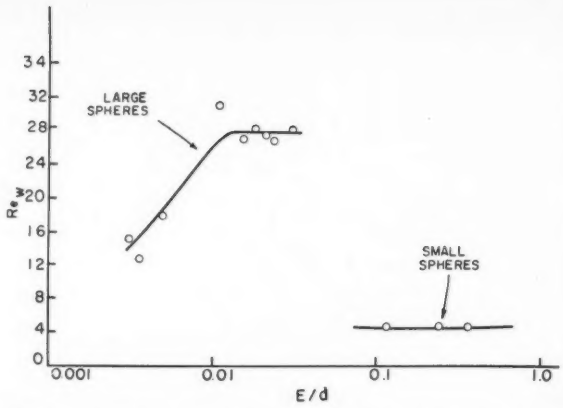

Figure 10—Minimum Reynolds Number for vortex formation for spheres fixed in an oscillating air column (Andrade).

The above work vividly points out the differences between the wake structures occurring in oscillating and steady motion, and similar differences which must influence the drag coefficient most likely occur at the pre-wake-forming Reynolds Numbers. In some of the experiments there was a steady motion superimposed over the oscillating fluid motion. This caused the upstream ring to diminish while the downstream vortex was distorted with increasing mean fluid velocity. Although the oscillation vortex system is gradually obliterated with increasing mean motion it still exerts an important influence, in turn distorting the steady state wake. Measurements of the drag forces in all these experimental studies, would have been very valuable but they could not be taken without difficult modifications to the equipment.

Very little is known about the effect of the oscillations on the lower critical Reynolds Number at which the wake shedding first begins. Carstens [57] seems to have uncovered a rather profound influence by a rough check made with a hot-wire anemometer during his oscillating table-tennis ball experiments which showed that no vortex separation had occurred even when the maximum Reynolds Number during the oscillation was as high as 3600. Schwabe's work indicates that this effect must be related to the period of the oscillation, the critical Reynolds Number increasing with the frequency. Keulegan and Carpenter [56] and McNown and Keulegan [104] suggest vortex development in oscillating systems should be correlated by the ratio of the time of flow in one direction T to the time taken to form a vortex T_s in the steady state case, the latter being obtained from the Strouhal Number Sr (see Part II), and they show that the parameter $(U_m T/d)$—which successfully correlated their data —is related to the (T/T_s) ratio through the relation:

$$(T/T_s) = (\mathrm{Sr})(U_m T/d) \qquad (20)$$

If repeated vortex shedding does occur in an unsteady flow, then the corresponding Strouhal Number most likely varies throughout the cycle and its relationship to the steady state Sr would not be a simple one. McNown and Keulegan found that the fluid distortion of the previous cycle inhibited the vortex formation and they underline the need for extensive investigation of the wake properties in unsteady systems.

Conclusions

Although the available experimental and theoretical information concerning the unsteady motion of a particle through a fluid is more deficient and in a cruder condition than that which is available for the corresponding steady state case, the following itemized generalizations are suggested:

(a) potential flow theory can be used to describe events only at the beginning of rectilinear accelerations as well as oscillatory motions involving very small amplitudes, and the added mass concept loses theoretical significance and practical utility if applied beyond this region;

(b) non-steady motion can cause very appreciable departures from the steady-state drag even for particulate movement in gases where the fluid-particle density ratio is extremely low;

(c) acceleration phenomena are correlated by reduced time parameters related to the number of particle diameters traversed since the initiation of the motion and are also dependent on the Reynolds Number describing the flow;

(d) the use of the total drag coefficient C_{DA} gives better results and has more theoretical justification than the summation of coefficients often employed;

(e) constant and varying acceleration rate experiments do not give similar drag coefficients and therefore the rate of change of the acceleration must be taken into account;

(f) an increase in wake turbulence caused by Reynolds Number increases or by surface roughening seems to decrease the effect of the acceleration on the drag; and

(g) the large decreases in drag noted in some acceleration experiments can not be explained in terms of present fundamental information which predicts increases in drag only and it is suggested that these data are influenced by phenomena other than acceleration.

From what is being said by the workers participating in the recent renewal of activity in this field, there will be many energetic inquiries made with a view to providing reliable quantitative drag values as well as a further insight into the fluid dynamics of unsteady motion.

Acknowledgments

The authors wish to express their appreciation for the continued assistance given to them by Librarians A. Finnemore and L. Lefebvre of the Pulp and Paper Research Institute of Canada, and P. Keir of McGill University, in obtaining the many papers reviewed in this series. L. B. Torobin is indebted to the Scientific Research Bureau, Trade and Commerce Department, Province of Quebec for three consecutive fellowships in support of his research program.

Nomenclature

Any consistent set of units may be employed. Those listed are merely illustrative.

a = wake length, ft.
C_D = steady state drag coefficient, dimensionless.
C_{DA} = total drag coefficient in accelerated motion, dimensionless, Equation (4).
C_D' = drag coefficient, dimensionless, Equation (6).
C_M = inertia coefficient, dimensionless, Equation (6).
d = body diameter, ft.
E = oscillation amplitude, ft.
f = oscillation frequency, cycles/sec.
F_g = body force due to gravity, lb. force.
g = local acceleration due to gravity, ft./sec.^{2}
h = distance between vortex centres, ft.
k_A = added mass coefficient, dimensionless, Equation (1).
k_1 = coefficient, (lb. force)(sec.)/ft., Equation (2).
k_2 = coefficient, (lb. force)(sec.^{2})/ft., Equation (2).
k_3 = viscous damping coefficient, (lb. force)(sec.)/ft., Equation (9).
k_4 = coefficient, dimensionless, Equation (15).
k_5 = coefficient, dimensionless, Equation (15).
L = cylinder length, ft.
L_p = characteristic particle length, ft.
L_W = wake length of flat plate, ft.
l' = axial distance between vortex centre and rear stagnation point, ft.
M = particle mass, lb.
M_A = added mass, lb., Equation (1).
N_1 = oscillation parameter $\sqrt{8\mu/\rho\omega}/d$, radians^{-1}.
N_2 = viscous damping ratio $k_3/3\pi\mu d$, dimensionless.
n = exponent, dimensionless.
R = steady state fluid drag force, lb. force.
R_A = acceleration fluid drag force, lb. force.
ΔR = supplementary drag force, lb. force.
Re = particle Reynolds Number, dimensionless.
Re_W = minimum Reynolds Number for wake formation, dimensionless.
Sr = Strouhal Number, dimensionless.
T = period of oscillation, sec.
T_θ = time parameter $(4\mu\theta/\rho d^2)$.
U_M = maximum relative velocity in oscillating cycle, ft./sec.
U_O = fluid velocity, ft./sec.
U_p = body velocity relative to fluid, ft./sec.
$|U_p|$ = positive numerical value of U_p, ft./sec.
V_p = particle volume, ft.^{3}
x = linear distance, ft.
θ = time, sec.
θ_B = reduced time parameter $\theta(U_p/d)^{1/2}$, dimensionless.
θ_S = reduced time parameter $U_p\theta/d$, dimensionless.
μ = absolute viscosity, lb./(sec.)(ft.)
ρ = fluid density, lb./ft.^{3}
ω = angular velocity, radians/sec.

References

(1) Torobin, L. B., and Gauvin, W. H., Can. J. Chem. Eng. **38**: 129 (1959).
(2) Torobin, L. B., and Gauvin, W. H., Can. J. Chem. Eng. **38**: 167 (1959).
(3) Lapple, C. E., and Shepherd, C. B., Ind. Eng. Chem. **32**: 605 (1940).
(4) Gilbert, M., Davis, L., and Altman, D., Jet Propulsion **25**: 26 (1955).
(5) Khudiakow, G. N., Izvest. Akad. Nauk S.S.S.R., Otdel. Tekh. Nauk **7**: 1022 (1953).
(6) Weidner, G., Forsch. Gebiete Ingenieurw. **21**: 145 (1955).
(7) Manning, W. P., Ph.D. Thesis, McGill University (1958).
(8) Hoffman, T. W., Ph.D. Thesis, McGill University (1959).
(9) Pasternak, I. S., Ph.D. Thesis, McGill University (1959).
(10) Bessel, F. W., "On the Incorrectness of the Reduction to a Vacuum Formerly Used in Pendulum Experiments". Berlin Academy (1826).
(11) Du Buat, C., "Principes d'Hydraulique". Paris (1786).
(12) Baily, F., Trans. Roy. Soc. London 399 (1832).
(13) McEwen, G. F., Phys. Rev. **23**: 492 (1911).
(14) Krishnayer, N. C., Phil. Mag. (6) **46**: 1049 (1923).
(15) Carstens, M. R., Trans. Am. Geophys. Union **33**: 332 (1952).
(16) Carstens, M. R., Am. Soc. Civil Engrs. **117**: 443 (1952).
(17) Allen, H. S., Phil. Mag. (5) **20**: 323 (1900).
(18) Schmidt, F. S., Ann. Physik (4) **61**: 633 (1920).
(19) Magnan, A., and St. Lague, A., Bulletin Technique No. 71 des Services Techniques de l'Aeronautique (1930).
(20) Cooke, G., Phil. Mag. (6) **39**: 350 (1920).
(21) Richardson, L. F., Phil. Trans. **223A**: 345 (1923).
(22) Hesselberg, T., and Birkeland, B. J., Beitr. z. Phys. d. freien Atmosph. **4**: 196 (1912).
(23) Cowley, W. L., and Levy, H., Adv. Ctee. Aero., Rep. and Mem. 612 (1918).
(24) Hirsch, P., Z.S. A.M.M. **3**: 93 (1923).
(25) Lunnon, R. G., Phil. Mag. 6th Ser. **47**: 173 (1924).
(26) Lunnon, R. G., Proc. Roy. Soc. (London) **110A**: 302 (1926).
(27) Lunnon, R. G., Proc. Roy. Soc. (London) **118A**: 680 (1928).
(28) Lunnon, R. G., Mining and Met. **10**: 333 (1929).
(29) Lunnon, R. G., Trans. Inst. Mining Engrs. **77**: 64 (1928).
(30) Lunnon, R. G., Chem. News 139 (1929).
(31) Torobin, L. B., Private Communication.
(32) Vagner, J. D., Pub. Scient. et Techniques du Ministere de L'air 110 (1937).
(33) Laws, J. O., Agric. Eng. **21**: 431 (1940).
(34) Laws, J. O., Trans. Am. Geophys. Union **22**: 709 (1941).
(35) Williams, G. C., Sc.D. Thesis M.I.T. (1942).
(36) Iverson, H. W., and Balent, R., J. Appl. Phys. **22**: 324 (1951).
(37) Keim, S. R., Proc. Amer. Soc. Civ. Engrs. **82**: HY 6 (J.Hr.Div.) Pap. 1113 (1956).
(38) Bugliarello, G., La Ricerca Scientifica **26**: 437 (1956).
(39) Ingebo, R. D., N.A.C.A. T.N. 3265 (1954).
(40) Ingebo, R. D., N.A.C.A. T.N. 3762 (1956).
(41) Fledderman, R. G., and Hanson, A. R., U. of Michigan Engineering Research Institute Report No. CM 667.
(42) Hanson, A. R., Proc. 2nd Midwestern Conf. on Fluid Mech. 415 (1952).
(43) Froessling, N., Gerlands Beitr. Geophys. **52**: 170 (1938).
(44) Luneau, J., Compt. Rend. **227**: 823 (1948).
(45) Luneau, J., Compt. Rend. **229**: 927 (1949).
(46) Luneau, J., Compt. Rend. **237**: 1140 (1953).
(47) Luneau, J., Compt. Rend. **243**: 334 (1956).
(48) Laird, A. D. K., and Johnson, C. A., Petrol. Tech. **8**: 65 (1956).
(49) Morison, J. R., O'Brien, M. P., Johnson, J. W., and Schaaf, S. A., J. Petrol. Technol. Am. Inst. Mining Engrs. **189**: 149 (1950).

(50) O'Brien, M. P., and Morison, J. R., Trans. Am. Geophys. Union **33**: 33 (1952).
(51) Morison, J. R., Proc. of Fourth Conference on Coastal Engineering, Council on Wave Research 340 (1953).
(52) Crooke, R. C., Beach Erosion Board T.M. 71 (1955).
(53) McNown, J. S., IX Congr. Internat. Mec. Appl., U. of Brusselles **3**: 124 (1957).
(54) Wiegel, R. L., Beebe, K. E., and Moon, J., Proc. Amer. Soc. Civ. Engrs. **83**: HY 2 (J. Hr. Div.) Pap. 1199 (1957).
(55) Borgman, L. E., Trans. Am. Geophys. Union **39**: 885 (1958).
(56) Keulegan, G. H., and Carpenter, L. H., J. Res. Nat. Bur. Stands. **60**: 423 (1958).
(57) Carstens, M. R., Trans. Am. Geophys. Union **33**: 713 (1952).
(58) Stelson, T. E., Ph.D. Thesis. Carnegie Institute of Technology (1952).
(59) Stelson, T. E., and Mavis, F. T., Proc. Amer. Soc. Civ. Engrs. **81**: 670 (1955).
(60) Polya, G., Proc. Nat. Acad. Sci. (U.S.A.) **33**: 218 (1947).
(61) Szego, G., Duke Journal of Math. **16**: 209 (1949).
(62) Basset, A. B., "A Treatise on Hydrodynamics". Cambridge (1888).
(63) Boussinesq, J., "Theorie Analytique de la Chaleur". Paris (1903).
(64) Oseen, C. W., "Hydrodynamik". Leipzig (1927).
(65) Tchen, C. M., "Mean Value and Correlation Problems Connected with the Motion of Small Particles Suspended in a Turbulent Fluid". Martinus Nijhoff, The Hague (1947).
(66) Pearcey, T., and Hill, G. W., Australian J. Phys. **9**: 18 (1956).
(67) Payne, R. B., J. Fluid Mech. **3**: 81 (1958).
(68) Kawaguti, M., J. Phys. Soc. Japan **8**: 747 (1953).
(69) Thom, A., Proc. Roy. Soc. (London) **141A**: 651 (1933).
(70) Goldstein, S., and Rosenhead, L., Proc. Camb. Phil. Soc. **32**: 392 (1936).
(71) Schwabe, M., Ingenieur Archiv **6**: 34 (1935).
(72) Blasius, H., N.A.C.A. T.M. 1256 (1950).
(73) Boltze, E., Ph.D. Thesis, Gottingen (1908).
(74) Sakurai, T., Proc. Phys. Math. Soc. Japan **21**: 632 (1939).
(75) Görtler, H., Ing.–Arch. **14**: 286 (1944).
(76) Görtler, H., Zschr. angew. Math. Mech. **25/27**: 145 (1957).
(77) Görtler, H., Arch. d. Math. **1**: 138 (1948).
(78) Schuh, H., Zeitschr. Flugw., **1**: 122 (1953).
(79) Rott, N., Quart. Appl. Math., **13**: 444 (1956).
(80) Yang, K. T., J. Appl. Mech. **26**: (Ser. E) 171 (1959).
(81) Lamb, H., "Hydrodynamics" Third Ed., Cambridge University Press, Cambridge (1906).
(82) Glauert, M. B., J. Fluid Mech. **1**: 97 (1956).
(83) Lighthill, M. J., Proc. Roy. Soc. (London) **224A**: 1 (1954).
(84) Mercier, R., Compt. Rend **246**: 698 (1958).
(85) Batailler, G., Compt. Rend. **242**: 452 (1956).
(86) Batailler, G., Compt. Rend. **242**: 2619 (1956).
(87) Andrade, E. N., Proc. Roy. Soc. (London) **134A**: 445 (1932).
(88) Andrade, E. N., Phil. Trans. **230A**: 413 (1932).
(89) Rayleigh, J. W. S., Lord, Phil. Trans. **175A**: 1 (1883).
(90) Schlichting, H., Phys. Z. **33**: 327 (1932).
(91) Carriere, M., J. Phys. et Radium **10**: 198 (1929).
(92) Carriere, M., J. Phys. et Radium **8**: 68 (1940).
(93) Skogem, M., Ph.D. Thesis, Physical Institute, U. of Oslo (1946).
(94) West, G. D., Proc. Phys. Soc. (London) **64**: 483 (1951).
(95) Westervelt, P. J., J. Acoust. Soc. Am. **25**: 60 (1953).
(96) Andres, J. M., and Ingard, U., J. Acoust. Soc. Am. **25**: 928 (1953).
(97) Andres, J. M., and Ingard, U., J. Acoust. Soc. Am. **25**: 932 (1953).
(98) Westervelt, P. J., J. Acoust. Soc. Am. **25**: 951 (1953).
(99) Holtsmark, J., Johnsen, I., Sikkeland, T., and Skavlem, S., J. Acoust. Soc. Am. **26**: 26 (1954).
(100) Raney, W. P., Corelli, J. C., and Westervelt, P. J., J. Acoust. Soc. Am. **26**: 1006 (1954).
(101) Skavlem, S., and Tjotta, S., J. Acoust. Soc. Am. **27**: 26 (1955).
(102) Lane, C. A., J. Acoust. Soc. Am. **27**:1082 (1955).
(103) Thrasher, R. W., and Westervelt, P. J., J. Acoust. Soc. Am. **28**: 796A (1956).
(104) McNown, J. S., and Keulegan, G. H., Proc. Amer. Soc. Civ. Engrs. **85**: EM 1 (J. Eng. Mech.): 1 (1959).

* * *

INDEX OF AUTHORS

THE CANADIAN JOURNAL OF CHEMICAL ENGINEERING—1959

Amberg, C. H., Peterson, W. S., and Madgwick, G. G.
"The Pyrolysis of a Heavy Crude Oil in a Fluidized Bed" Apr. 65

Becker, H. A.
"The Effects of Shape and Reynolds Number on Drag in the Motion of a Freely Oriented Body in an Infinite Fluid" ..... Apr. 85

Bellingham, A. I., and Simard, R.
"Sodium Hydroxide-Sodium Sulphate Stripping of Uranium from Amine Extracts" ..... June 113

Bogusz, E., Johnson, M., Kintner, R.C., and Warshay, W.
"Ultimate Velocity of Drops in Stationary Liquid Media" Feb. 29

Breitman, L., and Buckler, E. J.
"Distribution of Residence Times in Continuous Series of Mixing Zones" ..... Feb. 25

Buckler, E. J., and Breitman, L.
"Distribution of Residence Times in Continuous Series of Mixing Zones" ..... Feb. 25

Charles, M. E., and Russell, T. W. F.
"The Effect of the Less Viscous Liquid in the Laminar Flow of Two Immiscible Liquids" ..... Feb. 18

Cholette, A., and Cloutier, Leonce
"Mixing Efficiency Determinations for Continuous Flow Systems" ..... June 105

Clark, D. S., Lentz, C. P., and Murphy, D.
"Aeration in Tower-Type Fermenters" ..... Aug. 157

Cloutier, Leonce, and Cholette, A.
"Mixing Efficiency Determinations for Continuous Flow Systems" ..... June 105

Code, R. K., Plewes, A. C., and Pei, D. C.
"Some Thermodynamic Properties of the System Formic Acid-Water" ..... June 121

Dahlstrom, D. A., and Emmett, R. C.
"Liquid-Solid Separation Factors in Hydrometallurgical Leach Circuit Design" ..... Feb. 3

Duffie, J. A., and Lof, G. O. G.
"Solar Energy: Economics and Engineering Research at the University of Wisconsin" ..... Apr. 77

Embleton, T. F. W.
"Methods of Noise Control" ..... Feb. 37

Emmett, R. C., and Dahlstrom, D.A.
"Liquid-Solid Separation Factors in Hydrometallurgical Leach Circuit Design" ..... Feb. 3

Esplen, R. W., Mann, R. Singh, and Shemilt, L. W.
"Thermodynamic Properties of Some Organic Compounds. I. PVT Relationships and Calculated Thermodynamic Properties for Normal Butanol" ..... Aug. 142

Fan, Liang-Tseng, and Schwartz, Charles J.
"Note on Fluidization Onset in Beds of Rice and Wheat" Oct. 204

Gauvin, W. H., Pasternak, I. S., Torobin, L. B., and Yaffe, L.
"A Radioactive Tracer Technique for Particle Velocity Measurement in Solids-Gas Systems" ..... June 95

Gauvin, W. H., and Torobin, L. B.
Fundamental Aspects of Solids-Gas Flow. Part I: Introductory Concepts and Idealized Motion in Viscous Regime ..... Aug. 129

Gauvin, W. H., and Torobin, L. B.
"Fundamental Aspects of Solids-Gas Flow. Part II The Sphere Wake in Steady Laminar Fluids" ..... Oct. 167

Gauvin, W. H., and Torobin, L. B.
"Fundamental Aspects of Solids-Gas Flow. Part III. Accelerated Motion of a Particle in a Fluid" ..... Dec. 224

Ghosh, B., and Osberg, G. L.
"Heat Transfer in Water Spouted Beds" ..... Dec. 205

Govier, G. W., Russell, T. W. F., and Hodgson, G. W.
"Horizontal Pipeline Flow of Mixtures of Oil and Water" Feb. 9

Guthrie, D. A., and Scott, D.S.
"Removal of a Mist in a Fluidized Bed" ..... Oct. 200

Hedlin, C. P., and Hooper, F. C.
"Influence of the Presence of Vapor Diffusion from a Wetted Non-Adiabatic Boundary upon the Sensible Heat Transfer Between a Boundary Wall and a Gas Stream" Dec. 208

Hodgson, G. W., Govier, G. W., and Russell, T. W. F.
"Horizontal Pipeline Flow of Mixtures of Oil and Water" Feb. 9

Hooper, F. C., and Hedlin, C. P.
"Influence of the Presence of Vapor Diffusion from a Wetted Non-Adiabatic Boundary upon the Sensible Heat Transfer Between a Boundary Wall and a Gas Stream" Dec. 208

Johnson, A. I., and Madonis, J. A.
"Empirical Correlation of Azeotrope Data: An Extension of the Meissner-Greenfield Correlation" ..... Apr. 71

Johnson, M., Kintner, R. C., Warshay, W., and Bogusz, E.
"Ultimate Velocity of Drops in Stationary Liquid Media" Feb. 29

Johnson, A. I., and Raal, J. D.
"Liquid-Liquid Extraction with Association Effects" ..... Dec. 218

Kintner, R. C., Warshay, W., Bogusz, E., and Johnson, M.
"Ultimate Velocity of Drops in Stationary Liquid Media" Feb. 29

Kordbachen, Reza, and Tien, Chi.
"The Effect of Pressure on the Enthalpy of Gases" ..... Aug. 162

Lentz, C. P., Murphy, D., and Clark, D.S.
"Aeration in Tower-Type Fermenters" ..... Aug. 157

Li, James C. M., and Lu, Benjamin C.-Y.
"Note on Thermodynamic Consistency of Ternary Vapor-Liquid Equilibrium Data" ..... June 117

Lof, G. O. G., and Duffie, J. A.
"Solar Energy: Economics and Engineering Research at the University of Wisconsin" ..... Apr. 77

Lorenzo, A. P., Macrygeorgos, C. A., and Robinson, D. B.
"The Carbon Dioxide-Hydrogen Sulphide-Methane System. Part II. Phase Behavior at 40°F. and 160°F." ..... Dec. 212

Lu, Benjamin C.-Y., and Li, James C. M.
"A Note on Thermodynamic Consistency of Ternary Vapor-Liquid Equilibrium Data" ..... June 117

Lu, Benjamin C.-Y.
"Heats of Mixing and Vapor-Liquid Equilibrium Calculations" ..... Oct. 193

MacLeod, D. A., and Wheat, J. A.
"Tray Drying of Fine Powders" ..... Apr. 47

Macrygeorgos, C. A., Robinson, D. B., and Lorenzo, A. P.
"The Carbon Dioxide-Hydrogen Sulphide-Methane System. Part II. Phase Behavior at 40°F. and 160°F." ..... Dec. 212

Madgwick, G. G., Amberg, C. H., and Peterson, W. S.
"The Pyrolysis of a Heavy Crude Oil in a Fluidized Bed" Apr. 65

Madonis, J. A., and Johnson, A. I.
"Empirical Correlation of Azeotrope Data: An Extension of the Meissner-Greenfield Correlation" ..... Apr. 71

Mann, R. Singh, Shemilt, L. W., and Esplen, R. W.
"Thermodynamic Properties of Some Organic Compounds. I. PVT Relationships and Calculated Thermodynamic Properties for Normal Butanol" ..... Aug. 142

Mathers, W. G., and Winter, E. E.
"Principles and Operation of an Air Operated Mixer-Settler" ..... June 99

Mathur, K. B., Thorley, B., Saunby, J. B., and Osberg, G. L.
"An Analysis of Air and Solid Flow in a Spouted Wheat Bed" ..... Oct. 184

Mills, R. E.
"Development of Design Criteria for Biological Treatment of an Industrial Effluent Containing 2, 4-D Waste Water" ..... Oct. 177

Murphy, D., Clark, D. S., and Lentz, C. P.
"Aeration in Tower-Type Fermenters" ..... Aug. 157

Osberg, G. L., and Ghosh, B.
"Heat Transfer in Water Spouted Beds" ..... Dec. 205

Osberg, G. L., Thorley, B., Saunby J. B., and Mathur, K. B.
"An Analysis of Air and Solid Flow in a Spouted Wheat Bed" ..... Oct. 184

Pasternak, I. S., Torobin, L. B., Yaffe, L., and Gauvin, W. H.
"A Radioactive Tracer Technique for Particle Velocity Measurement in Solids-Gas Systems" ..... June 95

Pei, D. C., Code, R. K., and Plewes, A. C.
"Some Thermodynamic Properties of the System Formic Acid-Water" ..... June 121

Peterson, W. S., Madgwick, G. G., and Amberg, C. H.
"The Pyrolysis of a Heavy Crude Oil in a Fluidized Bed" Apr. 65

Plewes, A. C., Pei, D. C., and Code, R. K.
"Some Thermodynamic Properties of the System Formic Acid-Water" ..... June 121

Raal, J. D., and Johnson, A. I.
"Liquid-Liquid Extraction with Association Effects" ..... Dec. 218

Robinson, D. B., Lorenzo, A. P., and Macrygeorgos, C. A.
"The Carbon Dioxide-Hydrogen Sulphide-Methane System. Part II. Phase Behavior at 40°F. and 160°F." ..... Dec. 212

Russell, T. W. F., Hodgson, G. W., and Govier, G. W.
"Horizontal Pipeline Flow of Mixtures of Oil and Water" Feb. 9

Russell, T. W. F., and Charles, M.E.
"The Effect of the Less Viscous Liquid in the Laminar Flow of Two Immiscible Liquids" ..... Feb. 18

Saundy, J. B., Mathur, K. B., Osberg, G. L., and Thorley, B.
"An Analysis of Air and Solid Flow in a Spouted Wheat Bed" ..... Oct. 184

Schwartz, Charles J., and Fan, Liang-Tseng
"Note On Fluidization Onset in Beds of Rice and Wheat" Oct. 204

Scott, D. S., and Guthrie, D. A.
"Removal of a Mist in a Fluidized Bed" ..... Oct. 200

INDEX OF AUTHORS (Continued)

Shemilt, L. W., Esplen, R. W., and Mann, R. Singh
"Thermodynamic Properties of Some Organic Compounds. I. PVT Relationships and Calculated Thermodynamic Properties for Normal Butanol" ..... Aug. 142

Simard, R., and Bellingham, A. I.
"Sodium Hydroxide-Sodium Sulphate Stripping of Uranium from Amine Extracts" ..... June 113

Thorley, B., Saunby, J. B., Mathur, K. B., and Osberg, G. L.
"An Analysis of Air and Solid Flow in a Spouted Wheat Bed" ..... Oct. 184

Tien, Chi, and Kordbachen, Reza
"The Effect of Pressure on the Enthalpy of Gases" ..... Aug. 162

Torobin, L. B., Yaffe, L., Gauvin, W. H., and Pasternak, I. S.
"A Radioactive Tracer Technique for Particle Velocity Measurement in Solids-Gas Systems" ..... June 95

Torobin, L. B., and Gauvin, W. H.
"Fundamental Aspects of Solids-Gas Flow. Part I: Introductory Concepts and Idealized Motion in Viscous Regime" ..... Aug. 129

Torobin, L. B., and Gauvin, W. H.
"Fundamental Aspects of Solids-Gas Flow. Part II: The Sphere Wake in Steady Laminar Fluids" ..... Oct. 167

Torobin, L. B., and Gauvin, W. H.
"Fundamental Aspects of Solids-Gas Flow. Part III. Accelerated Motion of a Particle in a Fluid" ..... Dec. 224

Turner, A., Wellington, J. R., and Williams, L.
"Use of Lead in Chemical and Metallurgical Plant Construction" ..... Apr. 55

Warshay, W., Bogusz, E., Johnson, M., and Kintner, R.C.
"Ultimate Velocity of Drops in Stationary Liquid Media" ..... Feb. 92

Wellington, J. R., Williams, L., and Turner, A.
"Use of Lead in Chemical and Metallurgical Plant Construction" ..... Apr. 55

Wheat, J. A., and MacLeod, D. A.
"Tray Drying of Fine Powders" ..... Apr. 47

Wiles, D. R.
"Rate Control in the Hydrometallurgical Preparation of Uranium Dioxide" ..... Aug. 153

Williams, L., Turner, A., and Wellington, J. R.,
"Use of Lead in Chemical and Metallurgical Plant Construction" ..... Apr. 55

Winter, E. E., and Mathers, W. G.
"Principles and Operation of an Air Operated Mixer-Settler" ..... June 99

Yaffe, L., Gauvin, W. H., Pasternak, I. S., and Torobin, L. B.
"A Radioactive Tracer Technique for Particle Velocity Measurement in Solids-Gas Systems" ..... June 95

INDEX OF ARTICLES

THE CANADIAN JOURNAL OF CHEMICAL ENGINEERING—1959

Aeration of Tower-Type Fermenters ..... Aug. 157
Air Operated Mixer-Settler, Principles and Operation of an ..... June 99
Analysis of Air and Solid Flow in a Spouted Wheat Bed, An ..... Oct. 184
Azeotrope Data, Empirical Correlations of: An Extension of the Meissner-Greenfield Correlation ..... Apr. 71
Carbon Dioxide-Hydrogen Sulphide-Methane System, The, Part II: Phase Behavior at 40°F. and 160°F. ..... Dec. 212
Development of Design Criteria for Biological Treatment of an Industrial Effluent Containing 2, 4-D Waste Water ..... Oct. 177
Distribution of Residence Times in Continuous Series of Mixing Zones ..... Feb. 25
Drag in the Motion of a Freely Oriented Body in an Infinite Fluid, The Effects of Shape and Reynolds Number on ..... Apr. 85
Drying of Fine Powder Tray ..... Apr 47
Effect of the Less Viscous Liquid in the Laminar Flow of Two Immiscible Liquids, The ..... Feb. 18
Effect of Pressure on the Enthalpy of Gases, The ..... Aug. 162
Effects of Shape and Reynolds Number on Drag in the Motion of a Freely Oriented Body in an Infinite Fluid ..... Apr. 85
Effluent Containing 2, 4-D Waste Water, Development of Design Criteria for Biological Treatment of an Industrial ..... Oct. 177
Empirical Correlation of Azeotrope Data: An Extension of the Meissner-Greenfield Correlation ..... Apr. 71
Enthalpy of Gases, The Effect of Pressure on thee ..... Aug. 162
Fermenters, Aeration in Tower-Type ..... Aug. 157
Fluidization Onset in Beds of Rice and Wheat, Note on ..... Oct. 204
Fluidized Bed, Removal of a Mist in a ..... Oct. 200
Fluidized Bed, The Pyrolysis of a Heavy Crude Oil in a ..... Apr. 65
Flow Systems, Mixing Efficiency Determinations for Continuous ..... June 105
Fundamental Aspects of Solids-Gas Flow. Part I: Introductory Concepts and Idealized Motion in Viscous Regime ..... Aug. 129
Fundamental Aspects of Solids-Gas Flow. Part II: The Sphere Wake in Steady Laminar Fluids ..... Oct. 167
Fundamental Aspects of Solids-Gas Flow. Part III. Accelerated Motion of a Particle in a Fluid ..... Dec. 224
Heat Transfer in Water Spouted Beds ..... Dec. 205
Heats of Mixing and Vapor-Liquid Equilibrium Calculations ..... Oct. 193
Horizontal Pipeline Flow of Mixtures of Oil and Water ..... Feb. 9
Hydrometallurgical Leach Circuit Design, Liquid-Solid Separation Factors in ..... Feb. 3
Hydrometallurgical Preparation of Uranium Dioxide, Rate Control in the ..... Aug. 153
Influence of the Presence of Vapor Diffusion from a Wetted Non-Adiabatic Boundary upon the Sensible Heat Transfer Between a Boundary Wall and a Gas Stream ..... Dec. 208
Laminar Flow of Two Immiscible Liquids, The Effect of the Less Viscous Liquid in the ..... Feb. 18
Lead in Chemical and Metallurgical Plant Construction, Use of ..... Apr. 55
Liquid-Liquid Extraction with Association Effects ..... Dec. 218
Liquid-Solid Separation Factors in Hydrometallurgical Leach Circuit Design ..... Feb. 3
Methods of Noise Control ..... Feb. 37
Mixer-Settler, Principles and Operation of an Air Operated ..... June 99
Mixing Efficiency Determinations for Continuous Flow Systems ..... June 105
Mixing Zones, Distribution of Residence Times in Continuous Series of ..... Feb. 25
Mixtures of Oil and Water, Horizontal Pipeline Flow of ..... Feb. 9
Noise Control, Methods of ..... Feb. 37
Principles and Operation of An Air Operated Mixer-Settler ..... June 99
Pyrolysis of a Heavy Crude Oil in a Fluidized Bed ..... Apr. 65
Radioactive Tracer Technique for Particle Velocity Measurement in Solids-Gas Systems, A ..... June 95
Rate Control in the Hydrometallurgical Preparation of Uranium Dioxide ..... Aug. 153
Removal of a Mist in a Fluidized Bed ..... Oct. 200
Sodium Hydroxide-Sodium Sulphate Stripping of Uranium from Amine Extracts ..... June 113
Solids-Gas Flow, Fundamental Aspects of: Part I: Introductory Concepts and Idealized Motion in Viscous Regime ..... Aug. 129
Solids-Gas Flow, Fundamental Aspects of: Part II: The Sphere Wake in Steady Laminar Fluids ..... Oct. 167
Solids-Gas Flow, Fundamental Aspects of: Part III: Accelerated Motion of a Particle in a Fluid ..... Dec. 224
Solar Energy: Economics and Engineering Research at the University of Wisconsin ..... Apr. 77
Spouted Beds, Heat Transfer in Water ..... Dec. 205
Spouted Wheat Bed, An Analysis of Air and Solid Flow in a ..... Oct. 184
Thermodynamic Consistency of Ternary Vapor-Liquid Equilibrium Data, A Note on ..... June 117
Thermodynamic Properties of the System Formic Acid-Water, Some ..... June 121
Thermodynamic Properties of Some Organic Compounds. I. PVT Relationships and Calculated Thermodynamic Properties for Normal Butanol ..... Aug. 142
Tray Drying of Fine Powders ..... Apr. 47
Ultimate Velocity of Drops in Stationary Liquid Media ..... Feb. 29
Uranium from Amine Extracts, Sodium Hydroxide-Sodium Sulphate Stripping of ..... June 113
Use of Lead in Chemical and Metallurgical Plant Construction ..... Apr. 55
Velocity of Drops in Stationary Liquid Media, Ultimate ..... Feb. 29
Velocity Measurement in Solids-Gas Systems, A Radioactive Tracer Technique for Particle ..... June 95

MOTOR INSULATIONS

"MAGIC FORMULA" INSULATIONS ARE NO SUBSTITUTE FOR EXPERIENCED APPLICATION ENGINEERING!

Experience has proven that for correct, economical insulation there is still only one reliable approach: *experienced application engineering.*

Canadian Westinghouse continues to offer the *widest range* of motor insulations . . . to meet *every* application need. These insulations have been applied in all classes of Westinghouse motors, and their properties tested under the most varied conditions in industry. Among advanced Westinghouse motor insulations are:

ENCAPSULATED INSULATION . . . a new armament system for mush-wound motors. The stator is completely encapsulated in epoxy. The method used to apply the epoxy gives maximum cooling and protection to the coils. Encapsulated insulation is recommended for conditions subject to excess humidity . . . industrial concentration of chemicals . . . corrosive atmospheres . . . and where abrasives or other dusts collect on motor windings.

THERMALASTIC INSULATION . . . with the highest insulating qualities known for large motor stator coils. THERMALASTIC INSULATION has high thermal stability and effective heat dissipation. It is completely free of voids, and retains its elastic strength. Resists moisture, carbon black, dirt, oils, acids and alkalies. It is a mica-resin insulation, and the resins can be used as "building blocks." This enables Westinghouse to scientifically design the particular THERMALASTIC INSULATION that is most suitable for every class of service.

Insulation is a key factor in the cost of industrial drives. "Over-insulation" in standard service or "under-insulation" in severe conditions, are both ineffective and costly. Maximum economy is possible only when the insulation selected is suitable in every way to the conditions of service.

Westinghouse is the original pioneer in the development of motors . . . with more experience in motor insulation than any other manufacturer. Today, as always, Westinghouse motors are engineered, built—and insulated—to meet your applications *best!*

YOU CAN BE SURE... IF IT'S Westinghouse

59A150

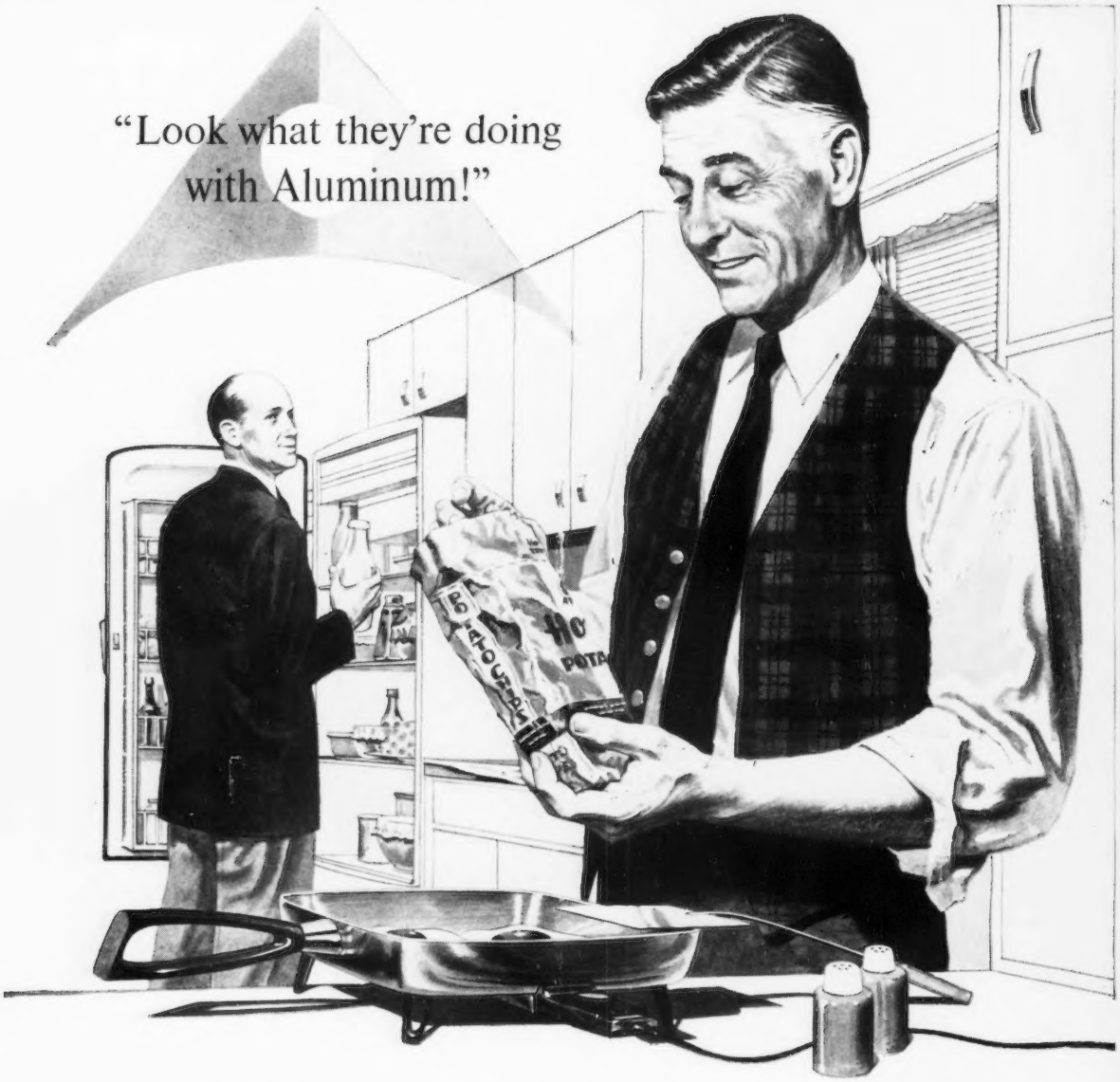

"Foil packaging and electric frying pans. Everyone's using aluminum. Why not in our products?"

Foil packaging that seals in freshness and flavour ...electrical appliances that are light, strong and convenient. Aluminum is everywhere. And no wonder. No other metal offers such a remarkable combination of qualities. And its uses continue to increase all the time with the development of new alloys, improved fabricating and welding techniques —and a growing consumer demand.

PERHAPS ALCAN ALUMINUM AND ALCAN "KNOW HOW" CAN HELP YOU IN YOUR BUSINESS.

ALCAN are the people to see about everything concerning aluminum. They are leaders in its development and set its standards of quality. ALCAN has over fifty years experience in aluminum and is the major source in Canada for aluminum sheet, wire, rod, bar, tubing, foil, extrusions, castings and ingot.

ALUMINUM COMPANY OF CANADA, LIMITED

An ALUMINIUM LIMITED Company

Quebec • Montreal • Ottawa • Toronto • Hamilton • Windsor • Winnipeg • Calgary • Vancouver

ALCAN

8772